








Neural Fields in Visual Computing and Beyond

<https://neuralfields.cs.brown.edu/>

Yiheng Xie^{1,2}  Towaki Takikawa^{3,4} Shunsuke Saito⁵  Or Litany⁴  Shiqin Yan¹ Numair Khan¹  Federico Tombari^{6,7}
James Tompkin¹  Vincent Sitzmann^{8†}  Srinath Sridhar^{1†} 

¹Brown University ²Unity Technologies ³University of Toronto ⁴NVIDIA ⁵Reality Labs Research ⁶Google ⁷Technical University of Munich
⁸Massachusetts Institute of Technology

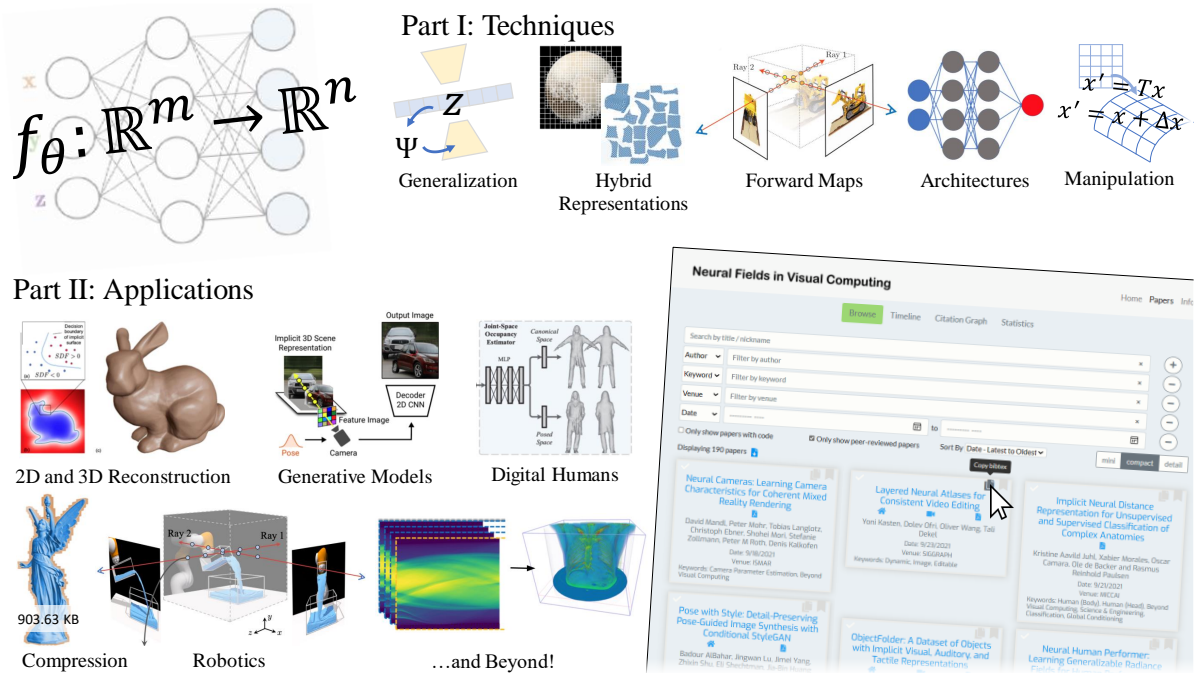


Figure 1: Contribution of this report. Following a survey of 251 papers, we provide a review of (**Part I**) techniques in neural fields across generalization, representation, forward maps, architectures, and manipulation, and of (**Part II**) applications in visual computing across 2D image processing, 3D scene reconstruction, generative modeling, digital humans, compression, robotics, and beyond. This report is complemented by a searchable and filterable community-driven website with bibliographic, bookmarking, and visualization features.

Abstract

Advances in machine learning have increased interest in solving visual computing problems using a class of coordinate-based neural networks that parameterize physical properties of scenes or objects across space and time. These methods, which we call **neural fields**, have seen widespread success in applications such as 3D shape and image synthesis, animation of human bodies, 3D reconstruction, and pose estimation. Rapid progress has led to numerous papers, but a formulation and review of the problems in visual computing has not yet emerged. We provide context, mathematical grounding, and a review of 251 papers in the literature on neural fields. In **Part I**, we focus on neural fields techniques by identifying common components of neural field methods, including different generalization, representation, forward map, architecture, and manipulation methods. In **Part II**, we focus on applications of neural fields to different problems in visual computing, and beyond (e.g., robotics, audio). Our review shows the breadth of topics already covered in visual computing, both historically and in current incarnations, and highlights the improved quality, flexibility, and capability brought by neural field methods. Finally, we present a [companion website](#) that contributes a living database that can be continually updated by the community.

CCS Concepts

• **Computing methodologies** → **Machine Learning; Artificial Intelligence;**

† Equal advising

1. Introduction

Visual computing involves the synthesis, estimation, manipulation, display, storage, and transmission of data about objects and scenes across space and time. In computer graphics, we synthesize 3D shapes and 2D images, render novel views of scenes, and animate articulating human bodies. In computer vision, we reconstruct 3D appearance, shape, and deformation and estimate the pose of objects. In HCI, we enable the interactive investigation of spacetime data. Beyond visual computing into adjacent fields like robotics, we use the structure of 3D scenes to plan and execute actions. Within these disciplines, **fields** are widely used to continuously parameterize an underlying physical quantity of an object or scene over space and time. For instance, fields have been used to visualize physical phenomena [Sab88], compute image gradients [SK97], compute collisions [OF03], or represent shapes via constructive solid geometry (CSG) [Eva15].

Across tasks in visual computing, we solve many different optimization problems, including via machine learning from large training data. One class of methods has gained significant attention since 2019: coordinate-based neural networks that represent a field. We refer to these methods as **neural fields**. Given sufficient parameters, fully connected neural networks can encode continuous signals over arbitrary dimensions at arbitrary resolution. Recent success with neural networks has caused a resurgence of interest in visual computing problems, leading to more accurate, higher fidelity, more expressive, and computationally cheaper solutions. This has let neural fields gain traction as a useful parameterization of 2D images [KAL*21], 3D shape [PFS*19, MON*19, CZ19], view-dependent appearance [SZW19, MST*20], and human bodies and faces [NMOG19, DLJ*20, SYMB21, YTB*21, RTE*21].

Such attention manifests as rapid progress and an explosion of papers (Figure 2), with a need to consolidate the discovered knowledge. However, a shared mathematical formulation to describe related techniques has not yet emerged, making it hard to communicate ideas and train students. Further, there is “*selective amnesia*” [SC21] of older or even concurrent work, causing research repetition. Finally, rapid progress makes any survey quickly out-of-date, requiring new summarization approaches.

We address these issues following a review of 251 papers both old and new: we define a neural field via fields of physical quantities, we provide a shared mathematical formulation across common techniques, we categorize, describe, and relate many applications, and we present a **living database** via a community website.

In **Part I**, we describe *neural field techniques* that are common across papers with a consistent notation and vocabulary. For instance, we identify and formalize recent hybrid discrete-continuous representations of neural fields, and techniques for learning priors such as local and global conditioning and meta-learning. Further, neural fields can be combined with a wide variety of differentiable forward maps, and we identify many such maps including surface and volume renderers and partial differential equations.

In **Part II**, we describe a broad cross-section of *applications of neural fields* to problems in visual computing. This lets us identify commonalities, connections, and trends across works representing shape and appearance of scenes and objects, including 3D recon-

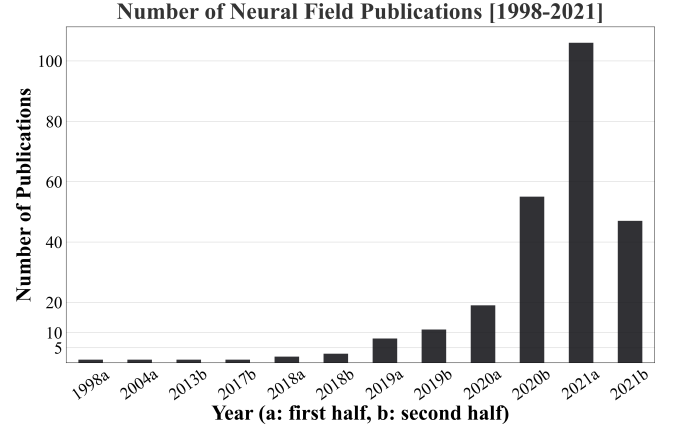


Figure 2: *Neural fields were proposed two decades ago, yet their growth in visual computing has been concentrated in the last two years with over two hundred papers.*

struction, digital humans, generative modeling, data compression, and 2D image processing. We also review works that solve tasks in adjacent communities including robotics (Section 11), medical imaging (Section 13.2), audio processing (Section 13.3), and wider physics-informed problems (Section 13.4).

Our **living database** is a [companion website](#) that provides search, filters, and visualizations to explore the works described in this report (Figure 1), along with simple bibliography and citation exporting. The website allows our community to submit new work in neural field that automatically update the database and are categorized into Part I and II taxonomies using keywords. The website is designed to require minimal maintenance, and we will release its source code to allow future reports and surveys to provide the same functionality.

In summary, neural field techniques are powerful and widely applicable to visual computing problems and beyond. This state-of-the-art report provides the mathematical formulation of techniques and discussion of applications to make sense of this exciting area, along with a community-driven website to continue to help researchers keep track of new developments in the future.

1.1. Background

Fields: We define a field following physics [FLS65, McM02]:

Definition 1 A *field* is a varying physical quantity of spatial and temporal coordinates.

We can represent a field as a continuous function $f : U \rightarrow \mathbb{R}^n$ that is defined for any coordinate \mathbf{x} in space and time $U \subseteq \{\mathbb{R}^m, t\}$ and that produces quantity \mathbf{q} . A *scalar field* has $n = 1$ and a *vector field* has $n > 1$ (Table 1). For instance, water pressure in a reservoir is a scalar field ($\mathbb{R}^3 \rightarrow \mathbb{R}$), and gravity is a vector field ($\mathbb{R}^3 \rightarrow \mathbb{R}^3$) around a particle of mass M governed by Newton’s law ($f(\mathbf{x}) = -GM\mathbf{x}/\|\mathbf{x}\|_2^3$). We can also define *tensor fields* to map space-time coordinates to higher-order *geometric tensors*, but we focus on scalar and vector fields.

In practice, the underlying field generation process may not have

Table 1: Examples of fields in physics and visual computing.

Examples	Field Quantity	Scalar/Vector	Coordinates
Gravitational Field	Force per unit mass (N/kg)	Vector	\mathbb{R}^n
3D Paraboloid: $z = x^2 + y^2$	Height z	Scalar	\mathbb{R}^2
2D Circle: $r^2 = x^2 + y^2$	Radius r	Scalar	\mathbb{R}^2
Signed Distance Field (SDF)	Signed distance	Scalar	\mathbb{R}^n
Occupancy Field	Occupancy	Scalar	\mathbb{R}^n
Image	RGB intensity	Vector	\mathbb{Z}^2 pixel locations x, y
Audio	Amplitude	Scalar	\mathbb{Z}^1 time t

a known analytic form. Thus, functions may be described by parameters Θ that are hand crafted, optimized, or learned. We denote such a field as producing $\mathbf{q} = \Phi(\mathbf{x}, \Theta)$. Furthermore, we often index sampled functions using discrete Cartesian values, such as at camera *pixels*, or choose discrete function parameterizations using *voxels* or discretized *level sets* because they are fast to query. However, discrete parameterizations are limited by the Nyquist sampling rate, causing high memory requirements for 3D tasks. Adaptive grids like octrees and k-d trees can reduce memory, but their generation can lead to costly combinatoric optimizations.

Neural Networks: A neural network connects many layers of artificial neurons to learn to non-linearly map a fixed-size input to a fixed-size output [LBH15]. Neural networks can approximate any function through their learned parameters (universal approximation theorem [KA03]). Common are feed-forward fully-connected neural networks, also called multi-layer perceptrons (MLPs). Since 2010, there has been significant interest in using neural networks with corresponding investment in hardware and software to support neural networks. This has significantly lowered the barrier to apply neural networks to a wide range of problems.

Neural Fields: A neural network can represent any field through its parameters Θ . Thus:

Definition 2 A *neural field* is a field that is parameterized fully or in part by a neural network.

Neural fields are both continuous and adaptive by construction. Unlike the memory required for discrete parameterizations that scales poorly with spatio-temporal resolution, the memory required for neural fields instead scales with the number of parameters of the neural network—often called its complexity. While other continuous parameterizations can represent large extents (for example, a Fourier series is a parameterization of a field), it is often difficult to know the required complexity ahead of time for efficient representation. Neural fields help to resolve this problem by using their parameters only where field detail is present. By their analytic differentiability, gradient descent, and over-parameterization [FC19], neural fields are effective at regressing complex signals through optimizations that are otherwise ill-posed.

Our definition of a neural field does not include neural networks whose co-domain has a spatial extent. These methods typically ingest a low-dimensional feature code as input and map it to a 2D or 3D grid of occupancy, RGB color, or other features [STH*19, LSS*19]. While the spatial grids output by these architectures can be seen as parameterizations of fields or can be used to locally condition a neural field (Section 3), the functions

parameterized by the neural network are not neural fields as they do not map a spatio-temporal coordinate to a feature.

Terminology: Within visual computing, neural fields have been called *implicit neural representations*, *neural implicits*, or *coordinate-based neural networks*. In neuroscience, the term *neural field* may describe theories about the organization and function of the brain [CbGPW14]. The term also describes a regular grid of neurons in a neural network [Lem92]. We exclude works in these alternative areas as they do not follow from our definition.

1.2. Related Surveys and Articles

Within visual computing, there are survey papers on specific areas like neural rendering [TFT*20] and 3D reconstruction [ZSG*18], and less formal attempts to gather related work in scene representations [NeRb, NeRa, Sit, NeRc]. Our broader survey aims to connect our different visual computing subcommunities and share findings.

Finally, neural fields are domain agnostic and can model arbitrary quantities beyond shape and appearance. Neural fields have been used extensively in computational physics via physics-informed neural networks (PINNs) [RPK19], with an existing survey [KKL*21]. To aid understanding, we make connections between methods for PINNs and for visual computing. Success in these areas leads us to anticipate wider application, with significant discoveries still outstanding.

Part I. Neural Field Techniques

A typical neural fields algorithm in visual computing proceeds as follows (Figure 3): Across space-time, we *sample coordinates* and feed them into a *neural network* to produce physical field values. Field values are samples from the desired *reconstruction domain* of our problem. Then, we apply a *forward map* to relate the reconstruction to the sensor domain, where supervision is available. Finally, we calculate the reconstruction error or *loss* that guides the neural network optimization process by comparing the reconstructed signal to the sensor measurement.

During this process, many problems affect our ability to successfully reconstruct the domain. To better understand and apply neural fields, we identify five classes of techniques, provide a mathematical formalization, and describe how they help us address these problems (Table 2). We can aid *generalization* from sparse sensor signals with conditioning and meta-learning techniques (Section 2). We can improve memory, computation, and neural network efficiency via *hybrid representations* using discrete data structures

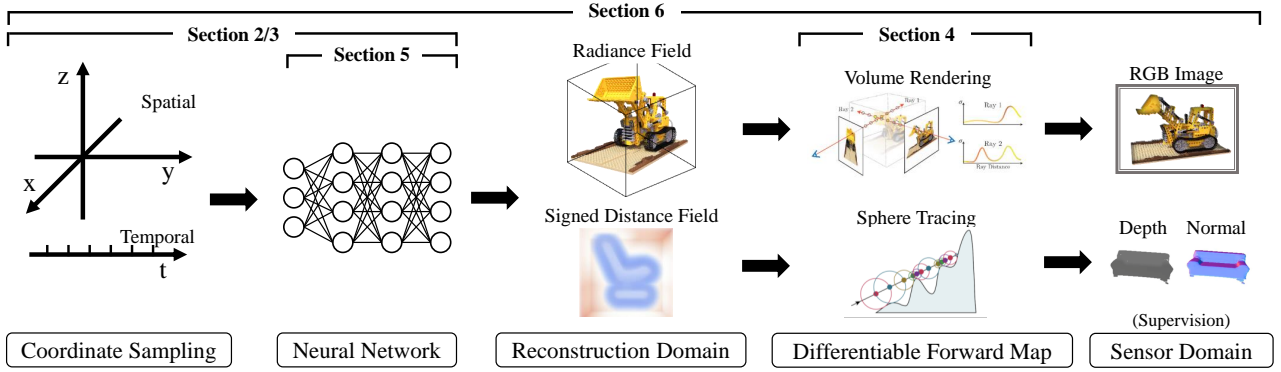


Figure 3: A typical feed-forward neural field algorithm. Spatiotemporal coordinates are fed into a neural network which predicts values in the reconstruct a domain. Then, this domain is mapped to the sensor domain where sensor measurements are available as supervision.

Class and Section	Problems Addressed
Generalization (Section 2)	Inverse problems, ill-posed problems, edit ability, symmetries.
Hybrid Representations (Section 3)	Computation & memory efficiency, representation capacity, edit ability.
Forward Maps (Section 4)	Inverse problems.
Network Architecture (Section 5)	Spectral bias, integration & derivatives.
Manipulating Neural Fields (Section 6)	Edit ability, constraints, regularization.

Table 2: The five classes of techniques in the neural field toolbox each addresses problems that arise in learning, inference, and control.

(Section 3). We can supervise reconstruction via differentiable *forward maps* that transform or project our domain (e.g., 3D reconstruction via 2D images; Section 4). With appropriate *network architecture* choices, we can overcome neural network spectral biases (blurriness) and efficiently compute derivatives and integrals (Section 5). Finally, we can *manipulate neural fields* to add constraints and regularizations, and to achieve editable representations (Section 6). Collectively, these classes constitute a ‘toolbox’ of techniques to help solve problems with neural fields.

2. Generalization

Suppose we wish to estimate a plausible 3D surface shape given a partial or noisy point cloud. We need a suitable prior over the surface in its reconstruction domain to *generalize* to the partial observations. A neural network expresses a prior via the function space of its architecture and parameters Θ , and generalization is influenced by the *inductive bias* of this function space (Section 5). Suppose also that we wish to vary our prior over the estimation of the plausible 3D shape depending on characteristics of the point cloud, or more broadly over characteristics of a reconstruction domain. For this, we can *condition* our neural field.

2.1. Conditional Neural Fields

A conditional neural field lets us vary priors via a conditioning latent variable \mathbf{z} . Observation-specific information can be encoded in the conditioning latent variable \mathbf{z} , while shared information can be encoded in the neural field parameters. Useful information separation is often called *disentanglement*. This also has implications beyond generalization. For instance, defining \mathbf{z} lets us interpolate or edit latent features from different observations, and condition across data types such as using speech to synthesize video of talking heads [GCL*21].

There are three components in a conditional neural field: (1) An encoder or inference function \mathcal{E} that outputs the conditioning latent variable \mathbf{z} given an observation \mathcal{O} : $\mathcal{E}(\mathcal{O}) = \mathbf{z}$. \mathbf{z} is typically a low-dimensional vector, and is often referred to as a *latent code* or *feature code*. (2) A mapping function Ψ between \mathbf{z} and neural field parameters Θ : $\Psi(\mathbf{z}) = \Theta$; (3) The neural field itself Φ . The encoder \mathcal{E} finds the most probable \mathbf{z} given the observations \mathcal{O} : $\arg \max_{\mathbf{z}} \mathbb{P}(\mathbf{z}|\mathcal{O})$. The decoder maximizes the inverse conditional probability to find the most probable \mathcal{O} given \mathbf{z} : $\arg \max_{\mathcal{O}} \mathbb{P}(\mathcal{O}|\mathbf{z})$.

We discuss different encoding schemes with different optimality guarantees (Section 2.1.1), both global and local conditioning (Section 2.1.2), and different mapping functions Ψ (Section 2.1.3).

2.1.1. Encoding the Conditioning Variable \mathbf{z}

Feed-forward Encoders / Amortized Inference: The latent code is generated via a learned inference function \mathcal{E} , typically parameterized as a feed-forward neural network (Figure 4, left). This provides no optimality guarantees; however, it is fast as inference requires only a single forward pass through a neural network, and the parameters in \mathcal{E} can encode priors. Examples of such encoders include PointNet [QSMG17] for point clouds, ResNet [HZRS16] for 2D images, or VoxNet [MS15] for voxel grids.

Auto-decoders: Auto-decoding methods lack a parametric encoder \mathcal{E} . Instead, latent codes \mathbf{z} are free variables to be directly optimized (Figure 4, right). Every training observation is initialized with its own latent code \mathbf{z}_i . To optimize a particular latent code \mathbf{z}_i , we map it to neural field parameters Θ via the mapping function Ψ , compute a reconstruction loss, and back-propagate that loss to \mathbf{z}_i to take a gradient descent step. At training time, the per-observation latent codes \mathbf{z}_i , the neural field Φ , and the conditioning function Ψ are jointly optimized. At test time, given a new observation $\hat{\mathcal{O}}$, we freeze parameters of Φ and Ψ and optimize the latent code $\hat{\mathbf{z}}$.

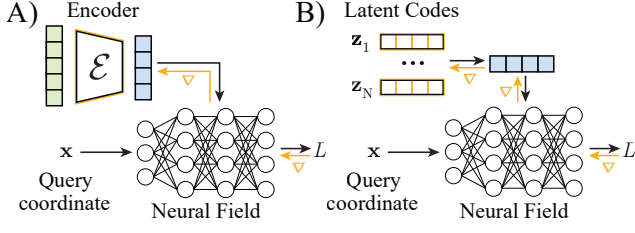


Figure 4: Inference: Encoding vs. Auto-decoding. (A) In amortized or encoder-based inference, encoder \mathcal{E} maps observations \mathcal{O} to latent variable \mathbf{z} . Parameters of \mathcal{E} are jointly optimized with the conditional neural field. (B) Auto-decoding lacks an encoder, and each neural field is represented by a separately-optimized latent code \mathbf{z}_i , which are jointly optimized with the conditional neural field. Gradient flow displayed in orange.

that minimizes the reconstruction error. Thus, auto-decoders solve $\arg \max_{\mathbf{z}} \mathbb{P}(\mathbf{z}|\mathcal{O})$ via first-order optimization; the optimization acts as encoder \mathcal{E} to map observations \mathcal{O} to latent variables \mathbf{z} .

Given the inference-time optimization, auto-decoding is significantly slower than a feed forward encoder approach. However, auto-decoding does not introduce additional parameters and does not make assumptions about observations \mathcal{O} . For instance, a 2D CNN encoder assumes \mathcal{O} to be on a 2D pixel grid, whereas an auto-decoder can ingest tuples of pixel coordinates and colors independently of their spatial arrangement. This can lead to robustness in certain out-of-distribution scenarios. For instance, in 3D reconstruction from images when observing a camera pose not in the training set, a convolutional encoder is constrained by the 2D geometry of its kernels whereas an auto-decoder is not [SZW19, LLS*21]. Due to these benefits, several works have adopted the auto-decoder approach [PFS*19, GSL*20, RTE*21, YWC*21, LZZ*21, JA21, TTG*21, SRF*21].

Hybrid approaches: These initialize \mathbf{z} with a forward pass of a parametric feed-forward encoder \mathcal{E} , then continue to optimize \mathbf{z} iteratively via an auto-decoder [MQK*21].

2.1.2. Global and Local Conditioning

In **global conditioning**, a single latent code $\mathbf{z} \in \mathbb{R}^n$ determines the entire neural field Φ across coordinate values. This is a desirable in representation learning when we want \mathbf{z} to be *compact*—to encode as much information as possible. However, a single low-dimensional latent code struggles to represent all parts of a complex reconstruction domain: A 3D scene with many objects that move independently has a combinatoric effect on the required global code. As such, global latent codes succeed at modeling class-specific distributions such as cars, aeroplanes, or human heads.

In **local conditioning**, many latent codes \mathbf{z} each have spatial extent over a local neighborhood in the space of \mathbf{x} . Thus, latent codes are a function of the input coordinate: $\mathbf{z} = g(\mathbf{x})$. Example g are discrete data structures like 2D raster grids [SHN*19, YYTK21, TY21], 3D voxel grids [PNM*20, LGL*20, JSM*20, CAPM20, CLI*20], surface patches [TTG*20], or orthographic 2D projections of 3D grids like floor maps [DBS*21, PNM*20]. Local conditioning enables reconstruction of 3D scenes with multiple moving objects, even if object configurations were not observed in training.

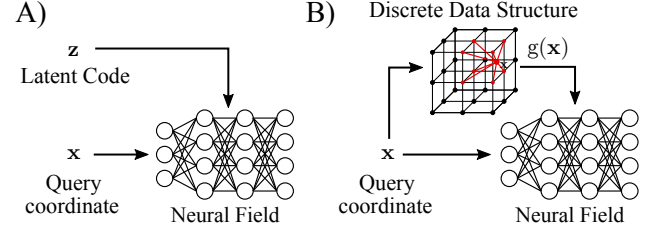


Figure 5: Local vs. Global Conditioning. (A) In global conditioning, a latent code \mathbf{z} defines the neural field across all input coordinates \mathbf{x} . (B) In local conditioning, a discrete data structure provides a coordinate-dependent latent code $\mathbf{z} = g(\mathbf{x})$ such that the neural network is coordinate-dependent. Figure adapted from [PNM*20].

Encoder \mathcal{E} only has to encode local properties in each \mathbf{z} . Further, the encoder can be built to preserve the spatial extent of the observation \mathcal{O} , such as 2D or 3D CNNs to extract features from images or discretized volumes. This can leverage encoder properties such as translation equivariance, granting better out-of-distribution generalization. Naturally, latent codes \mathbf{z} do not capture global scene information, which provides fewer constraints and less high-level manipulation control. Finally, in both types of conditioning, latent properties are meaningful only when the coordinate domain is explicit. For instance, locally with object-centric coordinates (Section 3) or globally with time-dependent coordinates [PSB*21].

Hybrid approaches: Global and local conditioning can be combined. For instance, for human face images, to attempt to disentangle a property that is shared across instances, like hair color, from another that is region specific, like wrinkling effects of aged skin.

2.1.3. Mapping \mathbf{z} to Neural Field Parameters Θ

Mapping latent variable \mathbf{z} to neural field parameters Θ always entails a function Ψ that computes neural field parameters: $\Theta = \Psi(\mathbf{z})$. Generalization ability, parameter count, and computational cost vary depending on the parameterization of Ψ and the choice of which parameters to predict.

Conditioning by Concatenation: Neural fields can be conditioned on latent variable \mathbf{z} by directly concatenating coordinate inputs \mathbf{x} with \mathbf{z} . Here, Ψ is implicitly a linear function that is parameterized by the respective weights in the first layer of Φ that map \mathbf{z} to the biases of the first layer of Φ [SCT*20, DPS*18, MGB*21].

Hypernetworks: Hypernetworks [HDL16] parameterize the function Ψ as a neural network that takes the latent code \mathbf{z} as input and outputs *all* neural field parameters Θ via a forward pass [SZW19, SMB*20, SRF*21, NWH21, CTT*21]. We can view this as a general form of conditioning: every other form of conditioning may be obtained from a hypernetwork by outputting only subsets of parameters Θ , by factorizing parameters of Φ via low-rank approximations or via additional scales and biases, or by varying Ψ architectures, such as using only a single linear layer. Early evidence suggests that full hypernetworks may more compactly encode information than concatenation-based methods given a large enough hypernetwork, suggesting that neural network grids can benefit from a more complex embedding of weights [GW20].

FiLM and other conditioning: Between conditioning via concatenation and full hypernetworks, one can condition an MLP

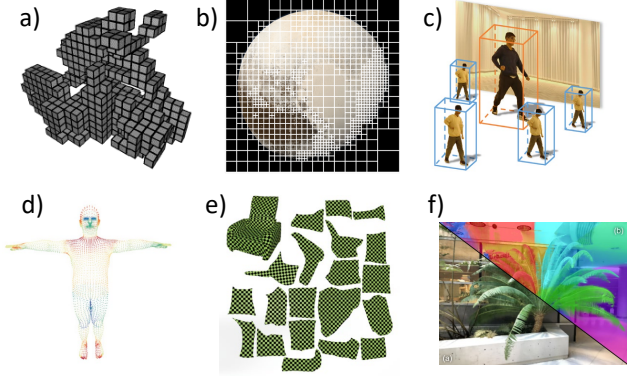


Figure 6: Examples of hybrid representations: a) neural sparse voxel grid [LGL*20], b) multi-scale voxel grid with neural 2D image compression [MLL*21], c) object bounding boxes with neural radiance fields [ZLY*21], d) mesh [PZX*21] e) atlas [GFK*18b], and f) Voronoi decomposition with neural radiance fields [RJY*21].

by predicting feature-wise transformations (FiLM) [DPS*18, CMK*21, MGB*21]. To FiLM-condition a neural field Φ , we use a network Ψ to predict a per-layer (and potentially per-neuron) scale γ and bias β vector from latent variables \mathbf{z} : $\Psi(\mathbf{z}) = \{\gamma, \beta\}$. The input \mathbf{x}_i to the i -th layer Φ_i is transformed as $\Phi_i = \gamma_i(\mathbf{z}) \odot \mathbf{x}_i + \beta_i(\mathbf{z})$. Another trade-off in the complexity of Ψ and the conditioning of Φ is to predict the factors of a low-rank decomposition of per-weight scales of the parameters of Φ [SIE21].

2.2. Gradient-based Meta-learning

An alternative to the conditional neural field approach is gradient-based meta-learning [FAL17]. Here, all neural fields in our target distribution are viewed as specializations of an underlying meta-network with parameters θ [SCT*20, TMW*21]. Specializations are obtained from fitting this meta-network to a set of observations \mathcal{O} , minimizing a reconstruction loss \mathcal{L} in a small number of gradient descent steps with step size λ :

$$\Theta^{j+1} = \Theta^j - \lambda \nabla \sum_{\mathcal{O}} \mathcal{L}(\Phi(\mathcal{O}; \Theta_i^j)), \quad \Theta_i^0 = \theta. \quad (1)$$

Similar to the auto-decoder framework in conditional neural fields, the inference function \mathcal{E} is implemented via an iterative optimization algorithm instead of a feed-forward neural network.

In a conditional neural field, the prior is expressed via the parameters of Ψ that enforce that the parameters of Φ lie in a low-dimensional space as defined by latent variable \mathbf{z} . However, in gradient-based meta-learning, the prior is expressed by constraining the optimization to not move the neural field parameters Θ too far away from the parameters of the meta-network θ . Gradient-based meta-learning enables fast inference, as only a few gradient descent steps are required to obtain Θ . As this does not assume a low-dimensional set of latent variables, in principle we retain the full expressivity of the neural field Φ .

3. Hybrid Representations

The second category of items in the neural field toolbox are **hybrid representations**. These combine neural fields with discrete data structures that decompose the input coordinate space to scale to large signals [RWG*13] (Figure 6). Discrete data structures are used extensively in visual computing, including regular grids, adaptive grids, curves, point clouds, and meshes. Discrete structures typically reduce computation, for instance using bounding volume hierarchies (BVHs) [RW80, MOB*21] to enables fast queries on hardware accelerators [PBD*10, WWB*14]. Discrete structures are also suitable for simulation such as via finite element methods, and can help in manipulation tasks (Section 6).

We accomplish spatial decomposition by storing some or all of the neural field parameters Θ_Φ in a data structure g . Given a coordinate \mathbf{x} , we query g to retrieve parameters Θ of the neural field. Two common approaches to how we map parameters Θ to data structure g are network tiling and embedding.

Network Tiling: A collection of *separate* neural fields Φ with disjoint parameters are tiled across the spatio-temporal input coordinates. Given a coordinate \mathbf{x} , we simply look up the network parameters in the data structure g :

$$\mathbf{q} = \Phi(\mathbf{x}, \Theta) = \Phi(\mathbf{x}, g(\mathbf{x})). \quad (2)$$

Embedding: We store latent variables \mathbf{z} in the data structure, as in Section 2.1.2. Neural field parameters Θ become a function of the *local* embedding $\mathbf{z} = g(\mathbf{x})$ via a mapping function Φ :

$$\mathbf{q} = \Phi(\mathbf{x}, \Theta) = \Phi(\mathbf{x}, \Psi(\mathbf{z})) = \Phi(\mathbf{x}, \Psi(g(\mathbf{x}))). \quad (3)$$

Tiling is a special case of embedding where Ψ is the identity function and \mathbf{z} is the parameters Θ . For design choice details of function Ψ , please refer to Section 2.

3.1. Defining g and its Common Forms

We define a discrete data structure g as a vector field that maps coordinates to quantities using a sum of Dirac delta functions δ :

$$g(\mathbf{x}) = \alpha_0 \delta(\mathbf{x}_0 - \mathbf{x}) + \alpha_1 \delta(\mathbf{x}_1 - \mathbf{x}) + \dots + \alpha_n \delta(\mathbf{x}_n - \mathbf{x}), \quad (4)$$

where coefficients α_i (scalar or vector) are the quantities stored at coordinates \mathbf{x}_i . For uniform voxels, the coordinates \mathbf{x}_i are distributed on a regular grid, whereas for a point cloud the coordinates \mathbf{x}_i are distributed arbitrarily. For network tiling, α_i is an entire set of network parameters Θ_i ; for embedding, α_i is latent variable \mathbf{z}_i .

Interpolation: The discrete data structure g may use an *interpolation scheme* to define g outside the coordinates \mathbf{x}_i of the Dirac deltas, such as nearest neighbor, linear, or cubic interpolation. If so, instead of Dirac deltas, function δ are basis functions of non-zero, compact, and local support. For instance, voxel grids are regularly combined with nearest-neighbor interpolation, where $g(\mathbf{x})$ is defined as α_i at the \mathbf{x}_i closest to \mathbf{x} .

3.1.1. Regular Grids

Regular grids such as pixels and voxels are widely used in visual computing. Their regularity makes them simple to index and convolve. Although simple, grids suffer from poor memory scaling in

high dimensions, and the Nyquist-Shannon theorem requires dense sampling for high-frequency signals. To overcome this, grids can be used with adaptive [MLL*21] and sparse schemes [CLI*20] such as hierarchical trees [LGL*20, TLY*21], for 3D data and for images [SHN*19] and tri-planar textures [PNM*20].

Grid tiling decomposes the coordinate domain to model larger-scale signals [JK20], require smaller neural networks per local region [RWG*13], make inference faster [RPLG21], and make neural fields suitable for parallel computing [SJK21]. Tiling may increase overfitting given sparse training data [HJKK21], and tile boundary artifacts are possible, though network parameter interpolation can be used to reduce boundary artifacts [DVPL21, MMNM21].

Grids of embeddings can similarly model larger-scale signals [CLI*20], enable the use of small neural networks [TLY*21], and benefit from interpolation [LGL*20]. Grids of embeddings can also be generated from other neural fields [MLL*21], generative models [ILK21], images [SSSJ20, TY21, CMK*21], or user input [HMBL21]. Please see Section 9 for a more detailed discussion.

3.1.2. Irregular Grids

Irregular structures can adaptively increase capacity in complex data regions, and so are not bound by the Nyquist-Shannon sampling limit. They may declare connectivity between coordinates explicitly such as in meshes, or implicitly such as in Voronoi cells. They too may also be organized into hierarchies, such as within a BVH or scene graph [GSRN21, OMT*21].

Point Clouds: Point clouds are a collection of sparse discrete coordinates. Each location can hold an embedding [TTG*20] or a network [RJY*21]. Although sparse in its support, point clouds can volumetrically define regions through Voronoi cells via nearest neighbor interpolation. For continuous interpolation, we can use Voronoi cells with natural neighbor interpolation [Sib81] or soft-Voronoi interpolation [WPLN*20].

Object-centric Representations: Object-centric representations are also a collection of points but where each has an orientation and a bounding box or volume [WSH*19]. Neural field parameters are stored at each point or at each vertex of the bounding volume, and can store embeddings [OMT*21] or networks [GFWF20, ZLY*21].

Mesh: Meshes are a common data structure in computer graphics with well understood properties and processing operations. For triangle meshes, embeddings can be stored on vertices [PZX*21] and interpolated with barycentric interpolation. For complex polygons, mean-value coordinates [Flo03] and harmonic coordinates [JMD*07] are options.

4. Forward Maps

In many applications, the *reconstruction domain* (how we represent the world) is different from the *sensor domain* (how we observe the world). Solving an *inverse problem* recovers the reconstruction from observations in the sensor domain, i.e., finding the parameters Θ of a neural field Φ given measurements from the sensor Ω .

We represent the (unknown) reconstruction as neural field $\Phi : \mathcal{X} \rightarrow \mathcal{Y}$ which maps world coordinates $\mathbf{x}_{\text{recon}} \in \mathcal{X}$ to quantities

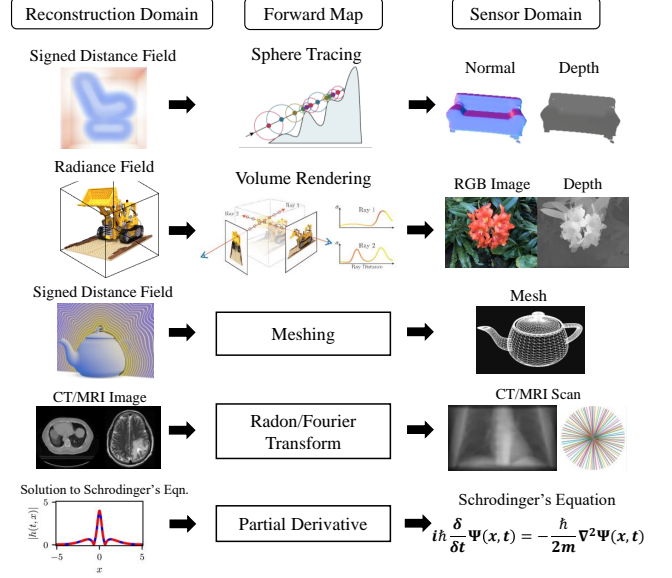


Figure 7: Forward maps relate reconstruction domains to sensor domains. Types of differentiable forward maps: a) sphere tracing [LZP*20], b) volume rendering [LSS*19, MST*20], c) meshing (e.g., marching cubes), d) Radon and Fourier Transformation [SPX21], e) partial derivatives [RPK]

$\mathbf{y}_{\text{recon}} \in \mathcal{Y}$. A sensor measurement is also a field $\Omega : \mathcal{S} \rightarrow \mathcal{T}$ which maps sensor coordinates $\mathbf{x}_{\text{sens}} \in \mathcal{S}$ to measurements $\mathbf{t}_{\text{sens}} \in \mathcal{T}$.

For instance, a 2D photograph from a camera is a field $\Omega : \mathbb{R}^2 \rightarrow \mathbb{R}$ representing irradiance. If we wish to model the reconstruction as a radiance field $\Phi : \mathbb{R}^5 \rightarrow \mathbb{R}$ of anisotropic photon flux, we need a mapping between Φ and Ω . We call such models **forward maps**.

A forward map is an operator $F : (\mathcal{X} \rightarrow \mathcal{Y}) \rightarrow (\mathcal{S} \rightarrow \mathcal{T})$, that is a mapping of functions. The forward map may depend on additional parameters, and may be composed with downstream operators such as sampling or optimization. We call a forward map *parameter differentiable* if for $\mathbf{y} = F(\Phi(\mathbf{x}))$ we can calculate the derivative $\frac{\partial \mathbf{y}}{\partial \theta}$, and *input differentiable* if we can calculate $\frac{\partial \mathbf{y}}{\partial \mathbf{x}}$.

Given a parameter differentiable forward map, we can solve the following optimization problem to recover the neural field Φ :

$$\min_{\Theta} \int_{(\mathbf{x}_{\text{recon}}, \mathbf{x}_{\text{sens}}) \in (\mathcal{X}, \mathcal{S})} \|F(\Phi(\mathbf{x}_{\text{recon}})) - \Omega(\mathbf{x}_{\text{sens}})\| \quad (5)$$

using differentiable programming and an algorithm such as stochastic gradient descent.

In the 2D image example, the forward map can be modeled with equations of radiative transfer, which integrate over a volumetric anisotropic vector field. Neural Radiance Fields (NeRFs) [MST*20] are one example that recovers isotropic density and anisotropic radiance fields from 2D image measurements. Even though many inverse problems are ill-posed with no guarantee that a solution exists or is unique, empirically forward maps help us to find good solutions in a variety of applications (Part II).

Problem	Sensor	Sensor Domain	Forward Module	Reconstruction Domain	Literature
3D Reconstruction	Digital Camera	Image (2D discrete array)	Rendering	Geometry, Appearance	[SHN*19, LSS*19, MST*20, YKM*20]
Geodesy Estimation	Accelerometer	Gravitational acceleration	$F = m\vec{a} = Gm_1m_2/\vec{r}^2$	Density (mass)	[IG21]
CT Reconstruction	X-ray Detector	Projection domain	Radon Transform	Density/Intensity	[SLX*21, ZIL*21, SPX21]
MRI Reconstruction	RF Detector	Frequency domain	Fourier Transform	Density/Intensity	[SPX21]
Audio Reconstruction	Microphone	Waveform	Fourier Transform	Spectrogram	[GCM*21]
Synthetic Aperture Sonar	Microphone	Waveform	Convolution (w/ PSF)	Point Scattering Distribution	[RBBJ]

Table 3: *Reconstruction: sensor domain, target domain, forward module. Detailed discussion on CT, MRI, Synthetic Aperture Sonar can be found in 13. RF: Radio Frequency, CT: Computed Tomography, MRI: Magnetic Resonance Imaging, PSF: Point Spread Function.*

4.1. Rendering

We define a *renderer* as a forward map which converts some neural field representation of 3D shape and appearance to an image. Renderers take as input intrinsic and extrinsic parameters, as well as the neural field Φ to generate an image. Extrinsic parameters define the translation and rotation of the camera, while intrinsic camera parameters define any other information for the image formation model such as field of view and lens distortion [HZ03]. Renderers often utilize a *raytracer* which takes as input a ray origin and a ray direction (*i.e.*, a single pixel from the camera model), and returns some information about the neural field. The information may be geometric like surface normals and intersection depth, or they may also aggregate or return some arbitrary features.

4.1.1. Ray-surface Intersection

If a neural field represents a shape’s surface, we can use several methods to obtain geometric information such as the surface normal and intersection point. For common shape neural fields representations such as occupancy and signed distance fields, ray-surface intersection amounts to a root finding algorithm. One such method is **ray marching**, which takes discrete steps on a ray to find the surface. Given the first interval, a method such as the Secant method can be used to refine the root within the interval. This method will fail to converge at the right surface if the surface is thinner than the interval which discrete steps are taken. Taking jittered steps can alleviate this by stochastically varying the step length and using supersampling [DW85]. Interval arithmetic can be used to guarantee convergence at the cost of iteration count [FSSV07]. In some cases, a neural network may be employed within ray marching to predict the next step [SZW19, NSP*21]. If the surface is Lipschitz-bounded (as is the case for signed distance fields), then **sphere tracing** [Har96] can efficiently find intersections with guaranteed convergence. Segment tracing [GGPP20] can further speed up convergence at the cost of additional segment arithmetic computation at each step.

These methods are all differentiable, but naively back-propagating through the iterative algorithm is computationally expensive. Instead, the surface intersection point alone can be used to compute the gradient [NMOG20, YKM*20]. If a hybrid representation is used, we can exploit a bounding volume hierarchy to speed up raytracing. In some cases, the data structure can also be rasterized onto the image to reduce the number of rays.

4.1.2. Surface Shading and Lighting

Once the ray-surface intersection point has been retrieved, we can calculate the radiance contribution *from* the point towards the cam-

era. This is done with a bidirectional scattering distribution function (BSDF) [CT82, BS12] which can be differentiable or be parameterized as a neural field [GN98]. To aggregate lighting contribution *to* the point, the most physically accurate method is to solve Kajiya’s rendering equation [Kaj86] with a multi-bounce Monte Carlo algorithm [PJH16]. However, this can be especially computationally expensive combined with a neural field.

To overcome this issue, approximations of incident lighting (related to precomputed radiance transfer) can be used. This include cubemaps [Gre86] or the use of spherical basis functions such as spherical harmonics [Gre03]. Neural fields can also be employed to approximate incident lighting [WPYS21]. In the case where the exact material properties or the lighting environment does not need to be modeled, a neural field with position and view direction as input can directly model the radiance towards the camera [MST*20].

4.1.3. Volume Rendering

The surface rendering equation cannot model scenes with inhomogeneous media such as clouds and fog. Even for scenes with opaque surfaces, inverse surface rendering has difficulty recovering high frequency or thin geometry such as hair and other meso-scale details because the gradients are only defined at surfaces. Instead of Kajiya’s rendering equation, volume rendering uses the *volume rendering integral* [KH84] based on the equations of radiative transfer [Cha13], for which the integral can be numerically approximated using quadrature (in practice, stochastic ray marching [PH89, MST*20]).

In a differentiable setting, under the assumptions of exponential transmittance, integration can be performed with a simple cumulative sum of samples across a ray, making backpropagation efficient and dense with respect to coordinates [MST*20]. This also propagates gradients throughout space, making the optimization easier. Non-exponential formulations exist [LSCL19, VJK21]; some are not physically accurate but work as an approximation.

One of the important factors in stochastic ray marching-based volume rendering is the number of samples. A higher sample count will mean more accurate models, but at the cost of computational cost and memory. Some approaches to mitigate this include using a coarse neural field model to importance sample [MST*20], using a classifier network [NSP*21], or using analytic anti-derivatives [LMW21].

4.1.4. Hybrid Volume and Surface Rendering

Many differentiable renderers try to combine the strengths of a opaque surface-based renderer and a volume renderer. Volume rendering is typically under-constrained due to the stochastic samples

taken on intervals, resulting in noise near surfaces. Surface rendering only provides gradients at the object surface, which do not smoothly propagate across the spatial domain.

We can combine approaches by re-parameterizing the implicit surface as a density field with soft boundaries using a Laplace distribution [YGKL21], a logistic density function [WLL*21], a Gaussian distribution, or a smoothed step function. We can also importance sample around the surface intersection point [OPG21].

4.2. Physics-informed Neural Networks

Partial differential equations (PDEs) are also powerful forward modules that map network outputs to gradient space supervision. Most of the works thus far have relied on a completely data-driven paradigm where additional constraints can be imposed by the choice of representation or implicit biases and invariance from the network architecture. Another class of methods, known as physics-informed neural networks (PINNs), use *learning bias* [KKL*21] which supervises boundary and initial values (from an incomplete simulation or observations) using a loss, and the rest of space by sampling or regularizing with equations of physics, typically partial differential equations (PDEs).

In visual computing, the PINN paradigm is often seen with signed distance functions [GYH*20]. One of the core properties of a SDF is that they satisfy the Eikonal equation. The boundary values are the point cloud \mathcal{X} which correspond to the 0-level set, and the Eikonal equation:

$$\|\nabla u(x)\| = \frac{1}{f(x)}, x \in \mathbb{R}^n \quad (6)$$

where in the special case when the $f(x) = 1$, $u(x)$ becomes an SDF. The Eikonal loss is therefore: $\mathcal{L} = \sum_{x \in \mathcal{X}} \|\|\nabla \Phi(x)\| - 1\|$.

PDEs are a natural description of the dynamics in the natural world. As such, a large collection of PDEs have been proposed in the discipline of physics, and naturally many of those PDEs have been used in conjunction with Neural Fields as PINNs. We refer readers to Karniadakis et. al for a much more comprehensive review of PINNs [KKL*21].

4.3. Identity Mapping Function

In some applications, the sensor domain may be the same as the reconstruction domain. In these cases, the forward model is the identity mapping function. The task is simply overfitting a neural field to data. Some examples are: supervising a neural signed distance field directly by ground-truth values [PFS*19], using neural fields to "memorize" images, or audio signals [SMB*20].

5. Network Architecture

The design choices that we make about the structure and components of a neural network have a significant impact on the quality of the field it parameterizes. Perhaps the simplest of these choices is the *network structure* itself, *i.e.*, how many layers are in the MLP, how many neurons are in each layer and so on. We assume that a reasonable structure with enough learning capacity has been chosen. We now discuss other design decisions that provide inductive biases for effectively learning neural fields.

5.1. Overcoming Spectral Bias

Real-world continuous signals are complex, making it challenging for neural networks to achieve high fidelity. Furthermore, neural networks are biased to fit functions with low spatial frequency [RBA*19]. Several designs address this shortcoming.

Positional Encoding: First proposed in the Natural Language Processing community, the coordinate input of the neural network may be transformed by a *positional encoding* $\gamma: \mathbb{R}^n \rightarrow \mathbb{R}^m$, which is a set of scalar functions $\gamma_i: \mathbb{R}^n \rightarrow \mathbb{R}$ which maps a coordinate vector $\mathbf{x} = [x_1, x_2, \dots, x_n]^T \in \mathbb{R}^n$ to a vector of embedded coordinates:

$$\gamma(\mathbf{x}) = [\gamma_1(\mathbf{x}), \gamma_2(\mathbf{x}), \dots, \gamma_m(\mathbf{x})]. \quad (7)$$

Sinusoidal functions are widely used to equip neural fields with the ability to fit high-frequency signals. Proposed by [ZBDB20a], they can be formally written as γ_i where:

$$\gamma_{(2i)}(x) = \sin(2^{i-1}\pi x), \quad (8)$$

$$\gamma_{(2i+1)}(x) = \cos(2^{i-1}\pi x). \quad (9)$$

These sinusoidal embeddings, also known as Fourier feature mapping, were subsequently popularized for the task of novel view synthesis [MST*20, TSM*20]. In the context of neural tangent kernels [JGH18], sinusoidal positional encoding can be shown to induce a kernel with a spatial selectivity that increases with the frequency of the functions ϕ_i . Positional encodings can thus also be seen as controlling the interpolation properties of a neural field.

Wang et al. [WLYT21] showed that the choice of the frequency of γ_i biases the network to learn certain, band-width limited frequency content, where lower encoding frequencies result in blurry reconstruction, and higher encoding frequencies introduce salt-and-pepper artifacts. For more stable optimization, one approach is to mask out high-frequency encoding terms at the beginning of the optimization, and progressively increase the high-frequency encoding weights in a coarse-to-fine manner [LMTL21, BHumRZ21]. SAPE proposed a more sophisticated masking scheme [HPG*21], which also allowed the encoding of spatially varying weights. Finally, alternative positional encoding functions ϕ_i have also been proposed [ZRL21, WLYT21]. In particular, [ZRL21] conducted a comprehensive study of various positional encoding functions.

Activation Functions: An alternative approach to enable the fitting of high-frequency functions is to replace standard, monotonic nonlinearities with periodic nonlinearities, such as the periodic sine as in SIREN [SMB*20] enabling fitting of high-frequency content. While a derivation of the properties of the neural tangent kernel is outstanding, some theoretical understanding can be gained by analyzing the relationships of the gradients of the output of the Neural Field with respect to neighboring coordinate inputs—for high frequencies of the sinusoidal activations, these gradients have been shown to be orthogonal, leading to an ability to perfectly fit values at any input coordinates without any interpolation whatsoever. It has been pointed out that positional encoding with Fourier features is equivalent to periodic nonlinearities with one hidden layer as the first neural network layer [BHumRZ21].

Warp Representation	Definition	Optimized Parameter	Related Works
Position	$\mathbf{x}' = \Phi(\mathbf{x})$	\mathbf{x}'	[CLCO*21, ASS21, NBB21]
Rigid Transformation	$\mathbf{x}' = \mathbf{T}\mathbf{x}$	\mathbf{T}	[NBB21, PSB*21, PSH*21]
Displacement	$\mathbf{x}' = \mathbf{x} + \Delta\mathbf{x}$	$\Delta\mathbf{x}$	[references below]
Velocity	$\mathbf{x}' = \mathbf{x} + \int_0^t \mathbf{v} dt$	\mathbf{v}	[NMOG19, BMSR20]
Discrete Cosine Transform	$\mathbf{x}' = (\frac{2}{T})^{1/2} \sum_{k=1}^K \phi_{\mathbf{x},k} \cos(\frac{\pi(2t+1)k}{2T})$	$\phi_{\mathbf{x},k}$	[WELG21]
Vector Field	$\mathbf{x}' = \mathbf{x} + t\mathbf{v}(\mathbf{x})$	$\mathbf{v}(\mathbf{x})$	[ANVL21]
Linear Blend Skinning (LBS)	$\mathbf{x}' = \sum_i \mathbf{T}_i w_i \mathbf{x}$	\mathbf{w}	[CZB*21, SYMB21, WMM*21]
Residual + LBS	$\mathbf{x}' = \sum_i \mathbf{T}_i w_i \mathbf{x} + \Delta\mathbf{x}$	$\Delta\mathbf{x}$	[LHR*21, TSTPM21]

Table 4: Spatial transformation of coordinates: x and x' are source and target coordinates; t is time; $\Phi: \mathbb{R}^m \rightarrow \mathbb{R}^3$ is neural deformation field; $\mathbf{T} \in \mathbb{R}^{4 \times 4}$ is rigid transformation matrix; $\Delta\mathbf{x} \in \mathbb{R}^3$ is displacement; $\mathbf{v} \in \mathbb{R}^3$ is velocity; $\phi_{\mathbf{x},k} \in \mathbb{R}$ is the k -th DCT coefficient at point \mathbf{x} ; T is number of frames; $K \in \mathbb{Z}^+$ is number of DCT coefficients; \mathbf{v} is flow vector; w_i are skinning weights given by the human body model. [references]: [LNSW21, PCPMMN21, YTB*21, TTG*21, PBT*21, WWZ*21, ZLY*21, GSKH21]

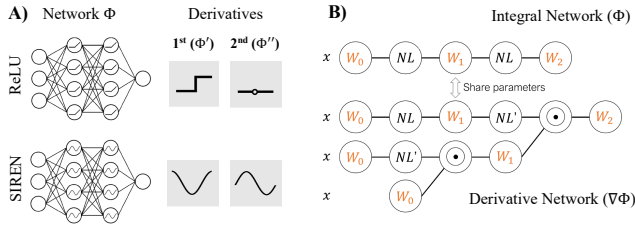


Figure 8: Derivatives and anti-derivatives of neural fields: A) Neural field derivatives depend on the non-linear activation function. ReLU yields piece-wise constant first derivatives and constant higher-order derivatives. Sinusoidal activations [SMB*20] yields (co-)sinusoidal derivatives. B) The computation graph of the derivative of a neural network can be easily assembled via automatic differentiation, and shares parameters with its anti-derivative. This enables solving of optimization problems that require supervising both a network and its gradients [SMB*20], as well as integration [LMW21]. NL denotes a non-linearity, NL' its derivative, and \odot denotes element-wise multiplication. Figures adapted from [SMB*20, LMW21].

5.2. Integration and Derivatives

Derivatives: A key benefit of neural fields is that they are highly flexible general function approximators whose derivatives $\nabla_{\mathbf{x}}\Phi(\mathbf{x})$ are easily obtained via automatic differentiation [G*89, BPRS18], making them attractive for tasks that require supervision of derivatives via PDEs. This, however, raises additional requirements in terms of the architecture of the MLP parameterizing the field. Specifically, the derivatives of the network must be nontrivial (*i.e.*, nonzero) to the degree of the PDE. For instance, to parameterize solutions of the wave equation — a second-order PDE — the second-order derivatives of the neural field must be nontrivial. This places restrictions on the activation function used in the network. For instance, ReLU nonlinearity has piece-wise constant first derivatives, and zero high-order derivatives, and so cannot generally parameterize solutions to the wave equation. Other common nonlinearities, such as softplus, tanh, or sigmoid, may address this issue, but often need to be combined with positional encodings to

parameterize high-frequency content of neural fields. Alternatively, the periodic sine may be used as an activation function [SMB*20].

Integrals: In some cases, we are further interested in solving an inverse problem where we measure the *derivative* quantity of a field, but are later interested in obtaining an expression for an integral over the neural field. In these cases, it is possible to sample the neural field and approximate the integral using numerical quadrature, as is often done for instance in volume rendering [MST*20]. However, the number of samples needed to approximate the integral may be arbitrarily large for a given accuracy.

While automatic differentiation is ubiquitous in deep learning, automatic integration is not well-explored. The seminal work AutoInt [LMW21] proposed to directly parameterize the *antiderivative* of the field as a neural field Φ . We may then instantiate the computational graph of its *gradient network* $\nabla_{\mathbf{x}}\Phi(\mathbf{x})$, and fit the gradient network to the given derivative values. At test time, a single integral can be calculated in one forward pass, as a consequence of the universal theorem of calculus.

6. Manipulating Neural Fields

While many data structures in visual computing have post-processing tools (e.g. smoothing a polygonal mesh), neural fields have limited tools for editing and manipulation, which significantly limits their use cases. Fortunately, this is an active area of research.

6.1. Input Coordinate Remapping

The simplest approach to editing neural fields is to transform its spatial or temporal coordinate inputs. A simple rigid translation of a neural field can be expressed as $g(x) = f(x+b)$. We discuss other more sophisticated coordinate remapping methods below (Table 4).

6.1.1. Spatial Transformation via Explicit Geometry

An intuitive solution for controlling shape or appearance neural fields is to leverage explicit shape information. For object modeling problems (Section 3.1.2), structural priors are often available

in the form of bounding boxes and coarse explicit geometry. Object bounding boxes offer a convenient, explicit handle to add and rigidly transform each object [ZLY*21, OMT*21, LGL*20].

For articulated objects, the kinematic chain offers explicit control over object geometry through its joint angles. At inference time, animating object geometry is achieved by changing joint angle inputs [MQK*21]. While this approach is effective for a small number of joints, it may introduce spurious correlations in case of long kinematic chains such as human body [LMR*15]. To avoid this issue, we can represent target shapes as the composition of local neural fields [GCS*20, DLJ*20]. Each local field is defined with respect to the joint transformations on a template mesh, and composed by max operation [DLJ*20] or weighted blending based on relative joint locations [SYZR21, NSLH21]. The primary drawback of articulated compositional neural fields is that each local field is independently modeled, often producing artifacts around joints with unobserved joint transformations. An alternative is to warp an observation space into a canonical space, where the reconstruction is defined, using the articulation of a template model [HXL*20, SYMB21]. The warping is commonly represented as linear blend skinning (LBS), where the deformations of surface is defined as the weighted sum of joint transformations. The blending weights are computed by a nearest-neighbor query on a template mesh [HXL*20] or learning as neural skinning fields [SYMB21, MZBT21, CZB*21, TSTPM21] (Table 4).

6.1.2. Spatial Transformation via Neural Fields

Unlike articulated objects with known transformations, modeling general dynamic scenes requires flexible representations that can handle arbitrary transformations. As target geometry and appearance are often modeled with neural fields, a continuous transformation of the field itself is a natural choice. Learning neural fields for spatial transformations is a highly under-constrained problem without 3D supervision [NMOG19]. This motivates the use of regularization loss terms based on physical intuitions:

- **Smoothness:** The first derivative of warp fields w.r.t. spatiotemporal coordinates should be smooth, assuming no sudden movements. This is necessary to constrain unobserved regions [GSKH21, PSB*21, TTG*21, DZY*21].
- **Sparsity:** 3D scenes generally contain large empty space. Thus, enforcing sparsity of the predicted motion fields avoids sub-optimal local minima [GSKH21, XHKK21, TTG*21, DZY*21].
- **Cycle Consistency:** If a representation provides both forward and backward warping (e.g. [GSKH21, WELG21, LNSW21], forward/inverse LBS [SYMB21, MZBT21]), we can employ cycle consistency as a loss function. Unlike other regularization terms, cycle consistency does not dampen the prediction as the global optimum should also satisfy this constraint.
- **Auxiliary Image-Space Loss:** Image-space information such as optical flows [LNSW21, XHKK21, DZY*21, GSKH21, WELG21] and depth maps [LNSW21, GSKH21, WELG21] can also be used in auxiliary loss functions.

6.1.3. Temporal Re-mapping

Conditioning the neural field on temporal coordinates allows time editing such as speed-up/slow-down ($\Phi(a \cdot t)$), offset ($\Phi(t + b)$), and reversal ($\Phi(-t)$) [ZLY*21, LNSW21].

6.2. Editing via Network Parameters

Neural fields can also be edited by directly manipulating the latent features or the learned network’s weights. These methods are task-agnostic, and are applicable to editing geometry, texture, as well as other physical quantities beyond visual computing. A subset of parameters can be selectively modified (e.g., geometry network, texture latent code). Network weight editing and manipulation methods include (see also Table 5):

- **Latent Code Interpolation/Swapping:** For neural fields conditioned on latent codes, interpolation or sampling in the latent space can change properties of the representation [CZ19].
- **Latent Code/Network Parameters Fine-Tuning:** After pre-training, we can fine-tune parameters to fit new, edited observations at test time. Editing may leverage explicit representations, such as sketches on 2D images [LZZ*21], or moving primitive shapes [HAESB20]. The neural field is coupled to the explicit supervision via differentiable forward maps.
- **Editing via Hypernetworks:** Hypernetworks can learn to map a new statistical distribution (e.g., a new texture style [CTT*21]) to a pre-trained neural field, by replacing its parameters.

Part II. Applications of Neural Fields

In Part II of this report, we review neural field works based on their application domain. The recent explosion of interest has seen neural fields being used for a wide range of problem in visual computing such as 3D shape and appearance reconstruction, novel view synthesis, human modeling, and medical imaging. Additionally, neural fields are increasingly being used in applications outside of visual computing including in physics and engineering. For each application domain, we limit our discussion to only neural field work while providing pointers to more traditional methods as context.

7. 3D Scene Reconstruction

The reconstruction of 3D content from real-world measurements is critical to a wide range of applications, such as entertainment, robotics and autonomous vehicles, and has consequently received a much attention. Unsurprisingly, the earliest work we are aware that uses neural fields was for 3D shape representation [LS04]. We use the term ‘3D content’ to refer to a broad range 3D scene properties including including geometry, appearance, materials, lighting, etc. for static and dynamic scenes. *Reconstruction* is the solution to an inverse problem, mapping available observations to a representation (e.g., 3D content). In the case of 3D reconstruction, available observations are discrete (due to sensors), often sparse (few images), incomplete (partial point clouds), residing in a lower dimension (2D images), or lack vital topological information (point clouds). The unique properties of neural fields make them an attractive parameterization of the solution space of such 3D scene

Task	Updated Parameter	Update Method	References
Geometry editing	Latent code	Backprop	DualSDF [HAESB20]
Shape removal/color editing	Network, latent code	Backprop	EditNeRF [LZZ*21]
Texture style transfer	Appearance network	Hypernetwork	Chiang et al. [CTT*21]
Facial expression animation	Latent code	Interpolation/swap	Gafni et al. [GTZN21], FLAME-in-NeRF [ASS21]
3D Geometry and/or texture editing	Latent code	Interpolation/swap	SRN [SZW19], DVR [NMOG20], IDR [YKM*20]
Camera view, lighting, time interpolation	Latent code	Interpolation/swap	XFields [BMSR20]
Diffuse albedo	Latent code	Interpolation/swap	NeRFactor [ZSD*21]

Table 5: Neural fields can be edited by directly changing network parameters such as weights and latent features. We list related work that performs editing through parameter editing.

reconstruction problems. In this section, we discuss all aspects of recovering, displaying, and editing 3D content while identifying what techniques from Part I they use.

7.1. Reconstruction of 3D Shape and Appearance

Reconstructing 3D Scenes with 3D Supervision: A large amount of work is focused on reconstructing representations of geometry in the form of signed distance functions or occupancy functions, given 3D supervision. An example of 3D supervision are point clouds: A point cloud is a set $\mathcal{X} \subset \mathbb{R}^3$ of 3D points. Point clouds often originate from sampling an underlying surface (e.g., with LiDAR). In addition to spatial location, they may contain information such as the surface normal, or appearance information.

A significant amount of work on neural fields for geometry reconstruction focuses on prior-based reconstruction, where generalization (see Section 2) is leveraged to learn a shape prior from data. AtlasNet [GFK*18b] proposed to represent 3D shapes via predicting a set of 2D neural fields that lift 2D local patch coordinates to 3D (an “atlas” of patches). Concurrently, FoldingNet [YFST18] proposed a similar idea but is not continuous. These patches were globally conditioned on a latent inferred from either a PointNet [QSMG17] or ResNet [HZRS16] encoder. IM-Net [CZ19] and Occupancy Networks [MON*19] proposed to represent 3D geometry via an occupancy function. Both proposed to generalize across ShapeNet [CFG*15] via global conditioning-via-concatenation, where the latent was regressed from either a CNN (from an image) or a PointNet encoder (from a point cloud). Concurrently, DeepSDF [PFS*19] proposed to represent 3D surfaces via their signed distance function, similarly generalizing across ShapeNet objects with global conditioning-via-concatenation, but performing inference in the auto-decoder framework instead. Fig. 9 visualizes the SDF representation. Even though these methods were proposed in conjunction with generalization, it is possible to overfit a DeepSDF or neural occupancy function on a single 3D shape.

AtlasNet was further extended [DGF*19] by learning elementary structures in a data-driven manner, and inferring point correspondences across instances. Four concurrent papers proposed to leverage local features stored in voxel grids for local conditioning (Section 2.1.2) to improve on prior-based inference. IF-Net [CAPM20], Chibane et al. [JSM*20], and Convolutional Occupancy Networks [PNM*20] use 3D CNNs or PointNet operating to process voxelized point clouds into embedding grids to lo-

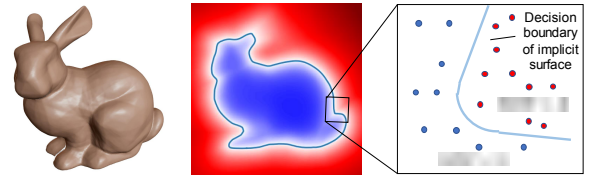


Figure 9: Neural fields for geometry commonly parameterize a surface as the level set of either an SDF [PFS*19], or occupancy function [MON*19, CZ19]. Figure adapted from DeepSDF [PFS*19].

cally parameterize an occupancy network or signed distance function, where conditioning proceeds via concatenation. In contrast, Chabra et al. [CLI*20] similarly leverages local conditioning from a 3D voxel grid, but infers the latent codes in the voxel grid via auto-decoding. CvxNet [DGY*20] proposes to represent a 3D shape as a composition of *implicitly defined* convex polytopes. LDIF [GCS*20] proposes to represent a 3D shape via a collection of local occupancy functions whose weighted sum represents the global geometry. Littwin et al. [LW19] infer an occupancy function via an image encoder and global conditioning via a hypernetwork.

Many methods aim to improve the quality of learned shapes. MetaSDF [SCT*20] was the first method to use gradient-based meta-learning (Section 2.1.3) for neural fields, using it to infer 3D signed distance functions from point clouds. Yang et al. [YWC*21] show that optimizing not only the embeddings but also the network weights regularized to be close to the original weights can better resolve ambiguities in unobserved regions. IGR [GYH*20] uses a neural field to parameterize an SDF, but instead of requiring ground-truth signed distance values in a identity forward map, they leverage a partial differential equation forward map via the Eikonal equation to learn SDFs from a point cloud. Atzmon et al. [AHY*19] derive analytical gradients of the 3D position of points on a level set with respect to the neural field parameters. SIREN [SMB*20] similarly learns an SDF with the Eikonal equation from oriented point clouds, but enables encoding of high-frequency detail by leveraging sinusoidal activations. Deep Medial Fields [RLS*21] proposes to parameterize geometry via its medial field, the local thickness of a 3D shape, enabling faster level-set finding and other applications. NGLoD [TLY*21] learns multiple level of details for SDFs with a compact hierarchical sparse octree of embeddings. SAL [AL20a] uses a neural field to parameterize SDF, and show that the SDF can be learned by optimizing against the unsigned distance function of the point cloud given

suitable initialization. SALD [AL20b] extends this with supervision of normals. Neural Splines [WTBZ21] use as input oriented point clouds and use kernel regression of the neural field to optimize for normal alignment. PIFu [YYTK21] performs prior-based reconstruction of geometry and appearance reconstruction by extracting features from images with a fully convolutional CNN, and, when querying a 3D point, projecting it on the image plane to use image features for local conditioning-via-concatenation. Concurrently, DISN [XWC*19] enhances single-view reconstruction by using a camera pose estimation that allows to project 3D coordinates onto the image plane and gather local CNN features. Combined with the global feature, the result is a more accurate SDF.

Differentiable Rendering: A major breakthrough in 3D reconstruction was the adoption of differentiable rendering (Section 4), which allowed reconstruction of 3D neural fields representing shape and/or appearance given only 2D images, instead of 3D supervision. This has significant implications since 3D data is often expensive to obtain, while 2D images are omni-present. A particularly important social implication is that non-experts can potentially become 3D content creators, without the barrier of specialized hardware or capture rigs. SRNs [SZW19] first proposed using a differentiable sphere-tracing based renderer to reconstruct 3D geometry and appearance from only 2D observations, and leveraged global conditioning via a hypernetwork and inference via auto-decoding to enable reconstruction of a 3D neural field of geometry and appearance from only a single image for the first time. Similar to DeepSDF, Occupancy Networks, and IM-Net, SRNs were designed to generalize, although they can be overfit given lots of 2D observations of a single 3D scene.

SDF-SRN [LWL20] enables learning an SRN from only a single observation per object at training time by enforcing a loss on the 2D projection of the 3D signed distance function. Kohli et al. [KSW20] leverages SRNs as a representation learning backbone for self-supervised semantic segmentation. Liu et al. [LSCL19] use a CNN to predict an embedding to parameterize occupancy, and a form of differentiable volume rendering to produce a silhouette. Liu et al. [LZP*20] similarly reconstruct 3D geometry from 2D images with differentiable sphere-tracing. DVR [NMOG20] represents geometry via an occupancy function, and finds the zero-level set via ray-marching, subsequently querying a texture network for RGB color per ray. Importantly, they derive an analytical gradient of the ray-marcher, which significantly reduces memory consumption at training time, but also requires ground-truth foreground-background masks. They demonstrate generalization across scenes via encoder-based conditioning, as well as overfitting on single scenes for high-quality, watertight 3D reconstruction.

NeuralVolumes [LSS*19] first proposed differentiable volume rendering, but leverages linearly interpolated voxel grids of color and density as a representation. Though the paper mentions parameterization of color and density functions as neural fields, this was only a part of the ablation studies, and reportedly under-performed a 3D CNN decoder in terms of resolution. cryoDRGN [ZBDB20b] implemented a differentiable volume renderer for the cryo-electron microscopy forward model to reconstruct protein structure from cryo-electron microscopy images, and proposed the positional encoding to allow fitting of high-frequency detail. Here, the neural

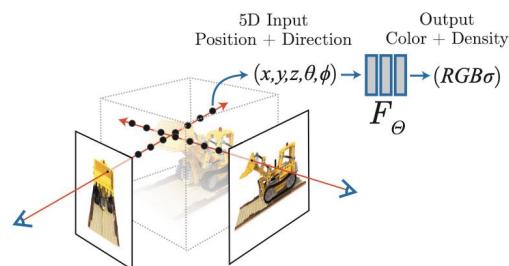


Figure 10: NeRF parameterizes a 3D scene as a 3D neural field mapping 3D coordinates to radiance and density, and can be rendered via volume rendering. Figure adapted from [MST*20].

field is parameterized in the Fourier domain, and the forward model is implemented via the Fourier slice theorem. NeRF [MST*20, TSM*20] combined volume rendering with a single ReLU MLP, parameterizing a monolithic neural field, and added positional encodings. By fitting a single neural field to a large number of images of a single 3D scene, this achieved photo-realistic novel view synthesis from only 2D images of arbitrary scenes for the first time. Fig. 10 displays the rendering process in NeRF. A significant amount of work has since proposed changes to the NeRF architecture. Nerf++ [ZRSK20] improves representation of unbounded 3D scenes via an inverted-sphere background parameterization. Reizenstein et al. [RSH*21] and Arandjelović et al. [AZ21] propose attention-based accumulation of samples along a ray. DoNeRF [NSP*21] proposes to jointly train a NeRF and a ray depth estimator for fewer samples and faster rendering at test time. [GKJ*21, YLT*21, RPLG21, HSM*21, LGL*20] propose various variants of local conditioning (without generalization, for overfitting a single scene) to speed up the rendering of NeRFs. Mip-NeRF [BMT*21] proposes to control the frequency of the positional encoding for multi-scale resolution control. NeRF—, BARF and iNeRF [WWX*21, LMTL21, YCFB*21] propose to back-propagate into camera parameters to enable camera pose estimation given a reasonable initialization.

PixelNeRF [YYTK21] and GRF [TY21] perform prior-based reconstruction by extracting features from images with a fully convolutional CNN, and, when querying a 3D point, projecting it on the image plane to use image features for local conditioning-via-concatenation, similar to PIFu and DISN [SHN*19, XWC*19]. With more context views, a similar approach can be used for multi-view-stereo-like 3D reconstruction [CXZ*21, CBLPM21]. NeRF-VAE embeds a globally-conditioned NeRF with encoder-based inference in a VAE-like framework [KSZ*21]. While volume rendering has better convergence properties than surface rendering and enables photorealistic novel view synthesis, the quality of the reconstructed geometry is worse, due to the lack of an implicit, watertight surface representation. IDR [YKM*20] leverages an SDF parameterization of geometry, a sphere-tracing based surface-renderer, and positional encodings to enable high-quality geometry reconstruction. Kellnhofer et al. [KJJ*21] distill an IDR model into a Lumigraph after rendering to enable fast novel view synthesis at test time. Concurrently, UNISURF [OPG21], NeuS [WLL*21], VolSDF [YGKL21] propose to relate the occupancy function of a volume to its volume density, thereby combining volume rendering and surface rendering, leading to improved rendering results

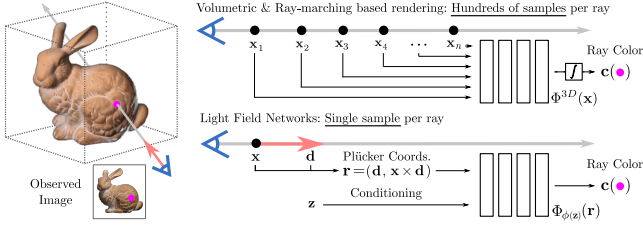


Figure 11: Instead of encoding a 3D scene with a 3D neural field that requires hundreds of samples along a ray to render, appearance & geometry may be encoded as a neural light field directly mapping an oriented ray to a color, enabling rendering with a single sample per ray, but requiring a multi-view consistency prior. Figure adapted from [SRF*21].

and better geometry reconstruction. Ray marching requires many samples along a ray to faithfully render complex 3D scenes. Even for relatively simple scenes, rendering requires hundreds or even thousands of evaluations of the neural scene representation per ray.

To overcome this limitation, we can parameterize the *light field* of a scene, which maps every ray to a radiance value. Light Field Networks [SRF*21] parameterize the 360-degree light field via a neural field, enabling real-time novel view synthesis with a single neural field sample per ray, and geometry extraction from the neural light field without ray-marching. Fig. 11 displays the difference between ray-marching and rendering in light fields. However, neural light fields are free to overfit to the training set so that interpolation between the observed viewpoints may not produce meaningful or accurate results. LFNs address this by learning a multi-view consistency prior while generalization across a dataset with global conditioning, hypernetworks, and inference via auto-decoding. Alternatively, an LFN may be trained for photo-realistic scenes by overfitting on *densely* sampled rays of a single scene. NeuLF [LLYX21] parameterizes forward-facing (not 360 degree) scenes via their light fields, overfitting on single scenes, and addresses multi-view consistency via enforcing similarity of randomly sampled views with the context views in the Fourier domain. NeX [WPYS21] parameterizes a set of multi-plane images as a 2D neural field, where the network inputs are pixel locations. Similar to light fields, rendering is computationally efficient in absence of ray-marching.

7.2. Reconstruction of Scene Material and Lighting

The goal of *material reconstruction* is to estimate the material properties of a surface or participating media from sparse measurements such as images. For opaque surfaces, this may be the parameters of a bidirection scattering distribution function (BSDF). For participating media, this may be phase functions. This is a difficult problem, because materials are diverse and create complex light transport effects. Even just for BSDFs, there is a whole taxonomy [MDH*20] of characteristic properties. In addition, to accurately estimating materials, we must also perform *lighting reconstruction* or have prior knowledge of the lighting.

The forward modeling of light transport involves surface rendering [Kaj86] and volume rendering [KH84] for participating media, which both equations having recursive integrals with no closed form solution for forward modeling. Approaches to inversely solve

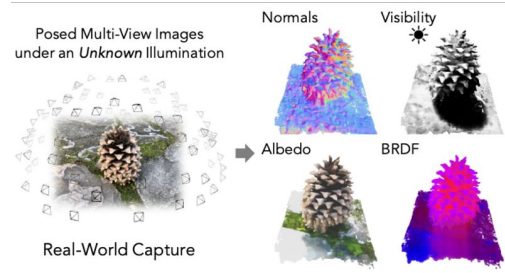


Figure 12: NeRFactor proposes neural fields for light visibility, BRDF, albedo, and surface normals, enabling re-rendering of 3D scenes under varying illumination and lighting following reconstruction. Figure adapted from [ZSD*21].

these equations differ in the degree of approximation they make. Because neural networks are general function approximators, they can be useful for estimating arbitrary functions and integrals that are hard to solve. Some methods reconstruct *appearance* as approximate incident radiance, and other methods attempt to separate appearance into *materials* via explicit scattering distribution functions and *lighting*, enabling applications such as relighting.

Neural Fields of Material Parameters: Many papers use a neural field to parameterize the parameter space of existing material models. Neural Reflectance Fields [BXS*20] can reconstruct both the SVBRDF and geometry by assuming a known point light source, and use a neural field which parameterizes density, normals, and parameters of a microfacet BRDF [WMLT07] with a volume rendering forward map with one bounce direct illumination. NeRV [SDZ*21] extends this to handle more varied lighting setups with an environment map and a one bounce indirect illumination forward map, along with an additional neural field which parameterizes visibility, but assume the environment map is known a priori. NeRD [BBJ*21] also use a neural field which parameterizes density, normals, and the parameters of a Disney BRDF model [CT82, BS12], but remove any assumptions on the lighting by using spherical gaussians to represent lighting of which the parameters are directly optimized. They do not model visibility or indirect illumination. PhySG [ZLW*21] also directly optimize spherical gaussians, but uses a neural field to parameterize an SDF and a Ward BRDF [War92] along with a hard-surface-based forward map to improve surface reconstruction accuracy. NeRFactor [ZSD*21] learns an embedding-based neural field of BRDF parameters as a prior on the material parameter space (Figure 12).

7.3. Dynamic Reconstruction

As well as novel-view synthesis, dynamic scene reconstruction also allows measurement, mixed reality, and visual effects. The challenges of modeling dynamic scenes are that the input data is even sparser in spacetime, and often no 4D ground-truth data are available. With careful design choices, the strong inductive bias of neural fields already helps. We review the existing approaches based on warp representation and how to embed temporal information. Please refer to Section 8 for dynamic reconstruction of 3D humans.

Embedding: Modeling temporally changing objects or scenes requires additional embedding that encodes frame informa-

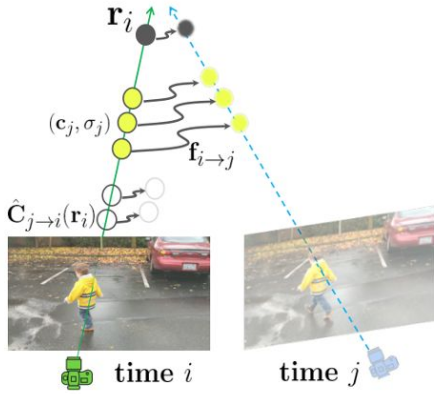


Figure 13: NSFF proposes novel time and view synthesis for dynamic scenes by reconstructing the 3D scene via a time dependent neural field. Figure adapted from [LNSW21].

tion [RBZ*20]. Occupancy Flow [NMOG19] models a dynamic component as a neural field conditioned by normalized temporal coordinates. Similarly dynamic scene reconstruction methods based on differentiable rendering often condition neural fields with temporal coordinates [XHKK21, LNSW21, PCPMN21, DZY*21]. Another approach is to jointly optimize per-frame latent code [PSB*21, LSZ*21, TTG*21, PSH*21, ALG*21] as embedding. While embedding based on temporal coordinates automatically incorporates temporal coherency as inductive bias, per-frame latent codes can enable the captures of more scene details.

Warp Representation: To model dynamic scene from limited input data, we can split the problem into modeling a scene in the canonical space and warping it into each time frame. In Section 6.1.2, we provide existing warp representations and common techniques to regularize the warp fields. While most approaches use the learned warping function as the final scene representation, several works use warp fields only for regularizing the predicted radiance fields [LNSW21, GSKH21]. Unlike other dynamic reconstruction approaches, where non-rigid complex warping is modeled by neural fields, STAR [YLSL21] models motion as a global rigid transformation to primarily focus on tracking of a foreground object.

8. Digital Humans

Human shape and appearance has received special attention in computer vision and graphics. The adoption of neural fields has produced unprecedentedly high-quality synthesis and reconstruction of human faces, bodies, and hands.

Face Modeling: The data-driven parametric morphable model was introduced by Blanz and Vetter [BV99]. However, these explicit representations lack realism and impose topological limitations making it difficult to model hair, teeth, etc. The expressiveness of fields, such as SDF and radiance fields, has made them an excellent candidate to address these limitations.

Given a collection of high-quality 3D scans, i3DMM [YTB*21] used coordinate-based neural networks that predict SDF and color to develop a 3D morphable head model with hair. Contrary to

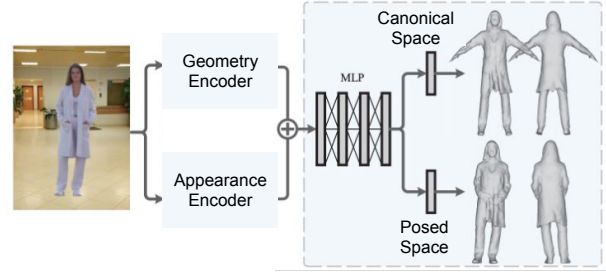


Figure 14: Yang et al. [YWM*21] jointly predict occupancy, skinning, and pose fields to animate reconstructed human avatars.

mesh-based representation, they learn an implicit reference shape as well as a deformation for each shape instance enabling editing abilities by disentangling color, identity, facial expressions, and hairstyle. Ramon et al. [RTE*21] use coordinate-based neural networks building upon IDR [YKM*20] to reconstruct a 3D head. To reduce the required amount of input images, a pre-trained DeepSDF-based latent space is used to regularize the test-time optimization. SIDER [CAMNS21] incorporates coarse geometric guidance via a fitted FLAME model [LBB*17] followed by implicit differentiation, enabling single-view optimization of facial geometry using SDF parameterized by a coordinate-based network.

While the aforementioned approaches focus on geometric accuracy assuming hard surfaces, NeRF have recently been adopted for photo-realistic view synthesis of human heads. Nerfies [PSB*21] utilizes a casual video footage captured with a moving hand-held camera to learn radiance fields and deformation fields of a human head. HyperNeRF [PSH*21] extends Nerfies by incorporating auxiliary hyper dimensions to handle large topological change.

Another line of works enable the semantic control of radiance fields by conditioning on head pose and facial expression parameters obtained from a 3D morphable face model [GTZN21, ASS21]. Supervised by multi-view video sequences, Wang et al. [WBL*21] use a variational formulation to encode dynamic properties in spatially varying animation codes stored in voxels. Notably, the above methods require per-subject training, and reconstruction from limited observations remains challenging. Several works show promise in few-shot, generalizable reconstruction by exploiting test-time fine-tuning [GSL*20] or pixel-aligned image features [RZS*21].

Body & Hand Modeling: Neural fields have demonstrated efficacy in 3D reconstruction of clothed humans from image inputs [SHN*19, SSSJ20, HCJS20, HXL*20, ZYLD21] or point clouds [CAPM20, BSTPM20a]. Due to substantial variations in shape and appearance of clothed human bodies, a global latent embedding does not lead to plausible reconstruction. PIFu [SHN*19] addresses this by introducing a coordinate-base neural network conditioned on pixel-aligned local embeddings. Its followup works also employ the framework of PIFu for human digitization tasks from RGB inputs [LXS*20, HCJS20, SJL*21, YWM*21, HZJ*21] or RGB-D inputs [LYP*20, YZG*21]. To further improve the fidelity of reconstruction, multi-level feature representations are shown effective [SSSJ20, CAPM20]. Yang et al. [YWM*21] jointly predict skinning fields and skeletal joints for animating the reconstructed avatars. Also, several works explicitly leverage a paramet-

ric body model such as SMPL [LMR*15] to improve robustness under different poses [ZYLD21] and to enable an animation-ready avatar reconstruction from a single image [HXL*20, HXS*21].

Human bodies are dynamic as they are both articulated and deformable. Several works show that providing the structure of human bodies significantly improves the learning of radiance fields [PZX*21, PDW*21, CZK*21, LHR*21]. Given a fitted body model to images, Neural Body [PZX*21] diffuses the latent embeddings on the body via sparse convolution, which are inputs to the neural field. Neural Actor [LHR*21] projects queried 3D points onto the closest point on the fitted body mesh, and retrieves latent embeddings on the UV texture map. A-NeRF [SYZR21] explicitly incorporates joint articulations, and learns radiance fields in the normalized coordinate space. In addition, as shown for face modeling, pixel-aligned local embeddings are highly effective to support novel-view rendering of unseen subjects [SZZ*21, KKCF21].

Template-mesh registration is another important task in body modeling. IP-Net [BSTPM20a] proposes to jointly infer inner body and clothing occupancy fields given input scans to aid registration. 3D-CODED [GFK*18a] proposes Shape Deformation Networks to fit a template to a target shape and infer correspondences. Halimi et al. [HIL*20] show template-based shape completion by conditioning the deformation field on the part and whole encoding. LoopReg [BSTPM20b] presents a self-supervised learning of dense correspondence fields on the predicted implicit surface to a template human mesh, which improves the robustness of surface registration. A continuous local shape descriptor for dense correspondence is proposed by Yang et al. [YLB*20]. Wang et al. [WGT21] model occupancy fields of input scans in an un-posed canonical space by predicting piece-wise transformation fields (PFT). Since shapes are modeled in the canonical space, we can perform template registration without self-intersection of different body parts.

Lastly, several recent works model a parametric model of human bodies [MZBT21, AXS21], clothed human [SYMB21, TSTPM21, PBT*21, WMM*21], hands [KYZ*20], or clothing [CPA*21] as neural implicit surfaces. One unique property of human body is the articulation with non-rigid deformations. Occupancy flow [NMOG19] models the non-rigid deformation of human bodies by warp fields. NASA [DLJ*20] presents articulated, per-body-part occupancy fields to model a pose-driven human body. However, articulated occupancy fields may suffer from artifacts around joints due to discontinuities. Another approach to handle articulation is jointly learning shapes in the un-posed canonical space and transformations from the canonical space to the posed space [SYMB21, MZBT21, PBT*21, CZB*21], leading to continuous deformations around body joints. The transformation can be modeled as warp fields (Section 6.1.2) in the form of displacements [PBT*21] or Linear Blend Skinning weights [SYMB21, MZBT21, CZB*21, TSTPM21, WMM*21].

9. Generative Modeling

Assuming a dataset of samples drawn from a distribution $\mathbf{y} \sim \mathcal{D}$, generative modeling defines a latent distribution \mathcal{Z} , such that every sample \mathbf{y} can be identified with a corresponding latent $\mathbf{z} \sim \mathcal{Z}$. The mapping from \mathcal{Z} to samples from \mathcal{D} , is performed via a learned generator \mathbf{g} , parameterized as a deep neural network, $\mathbf{g}(\mathbf{z}) = \mathbf{y}$.

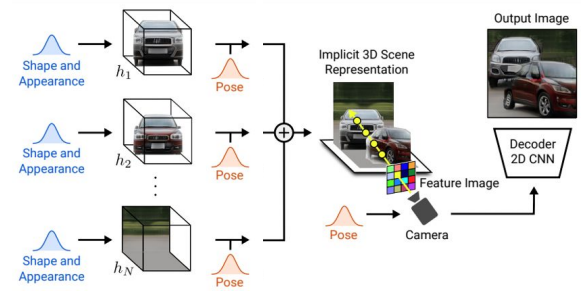


Figure 15: By leveraging object-centric local conditioning, *Giraffe* [NG21b] learns a generative model that learns to disentangle a scene into separate 3D object representations.

Neural fields provide greater flexibility for generative modeling because their outputs can be sampled at arbitrary resolutions, and because input samples can be shifted by simply applying transforms to the input coordinates. Each sample \mathbf{y} is associated with a neural field Φ that can be densely queried across the coordinate domain to obtain the sample \mathbf{y} . Consistent with the notation in Section 2, latent variables \mathbf{z} can either *globally* or *locally* condition the neural field Φ , yielding a conditional neural field $\Phi(\mathbf{x}, \mathbf{z})$.

Generative Modeling of Images: In generative modeling of images, samples \mathbf{y} are images, and we assume that there exists a distribution \mathcal{D} of “natural” images. The neural field Φ maps 2D pixel coordinates to RGB colors, $\Phi : \mathbb{R}^2 \rightarrow \mathbb{R}^3$. Bond-Taylor and Willcocks [BTW21] adopt a single-step gradient-based meta-learning approach for variational inference of images with a SIREN [SMB*20] decoder. INR-GAN [SIE21] leverage global conditioning and a hypernetwork predicting a low-rank decomposition of the weight matrices of Φ . CIPS [ADK*21] and StyleGAN3 [KAL*21] leverage global conditioning with a FiLM-style conditioning. The latter three approaches leverage Fourier Features [TSM*20] to allow generation of high-frequency content. At the time of writing this report, neural field-based image generative models are the state-of-the-art.

Generative Modeling of 3D Shape: IM-Net [CZ19] generatively models 3D shapes by parameterizing a neural field of occupancy $\Phi : \mathbb{R}^3 \rightarrow \mathbb{R}^1$ and globally conditioning on latents \mathbf{z} via concatenation. Similarly, Occupancy Networks [MON*19] employ a variational autoencoder (VAE) to learn a generative model of 3D occupancy fields. DeepSDF, on the other hand, learns the distribution of SDFs by directly optimizing shape latent codes in the spirit of Generative Latent Optimization [BJLPS17] without encoders.

Generative Modeling of 3D Shape and Appearance: Instead of directly modeling the distribution of images, neural fields can parameterize distributions over 3D shape and appearance given only an image dataset. The neural field $\Phi : \mathbb{R}^3 \rightarrow \mathbb{R}^n$ then maps a 3D coordinate to a quantity that encodes shape and appearance. This is combined with a neural forward rendering model that renders an image given camera parameters.

GRAF [SLNG20] first adapted this via a neural radiance field and volume rendering forward model, globally conditioned via concatenation. Chan et al [CMK*21] improve upon GRAF by using

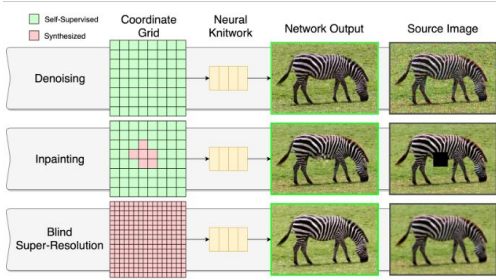


Figure 16: *Neural Knitworks* [CCA*21] utilizes patch based 2D neural fields for image processing tasks: denoising, blind super-resolution and inpainting. See Section 10

sinusoidal activation functions [SMB*20] in the MLP, and global FiLM conditioning. StyleNeRF [Ano22] combine StyleGAN-style FiLM conditioning with accelerated rendering techniques such as low-resolution rendering and 2D upsampling. By leveraging local conditioning via object-centric compositions (see Section 3), GIRAFFE [NG21b] generates an output image as the composition of multiple neural fields, which allows control over shape, appearance and scene layout. CAMPARI [NG21a] train an additional camera generator along with the 3D volume generator which generalizes to complex pose distributions.

Multi-modal generative modeling. An advantage of neural fields is that they are, in principle, agnostic to the signal they parameterize. Du et al. [DCTS21] combine global conditioning, the auto-decoder framework, and latent space regularization to learn multi-modal (such as audio-visual) manifolds.

10. 2D Image Processing

A compelling feature of 2D neural fields is the ability to represent continuous images. The first neural network to parameterize an image was demonstrated by Stanley et al. [Sta07]. These networks were not fit via gradient descent, instead relying on architecture search in a genetic algorithm framework, and could thus not represent images with fine detail. Fitting natural images with neural fields in a modern deep-learning framework was first demonstrated by SIREN [SMB*20] and FFN [TSM*20], and by [SCA19] who decomposed the image into continuous vector layers. Unlike grid-based convolutional architectures, continuous images can be sampled at any resolution.

As a result, they have been used for a variety of image processing tasks described below.

Image-to-image translation techniques take an input image and map it to another image that preserves some representation of the content. Common tasks include image enhancement, super-resolution, denoising, inpainting, semantic mapping and generative modeling [Izze17]. Since this task requires learning a prior from data, an encoder-decoder architecture is often used, where the encoder is a convolutional neural network, and the decoder is a locally conditioned 2D neural field (Section 2).

Chen et al. [CLW21] propose such a locally conditioned neural field with a convolutional encoder for the task of image super-resolution, naturally leveraging the resolution independence of the

neural field decoder. Shaham et al. [SGZ*21] leverage a convolutional encoder to produce a low-resolution, 2D feature map from an input image, which is then upsampled with nearest-neighbor interpolation to locally condition a decoder neural field. They demonstrate speedups for a variety of image-to-image translation tasks, such as segmentation and segmentation-to-RGB image as compared to the fully convolutional baseline. Neural Knitworks [CCA*21] discretize the 2D space into patches to introduce the appropriate receptive field, for inpainting, super-resolution, and denoising. CIPS [ADK*21] proposes an image synthesis architecture whose input pixels coordinates are conditionally-independent given latent vector \mathbf{z} . Global information is given by \mathbf{z} , which is used by a hypernetwork to modulate the neural field weights. INR-GAN [SIE21] similarly uses a hypernetwork and latent code \mathbf{z} to modulate the linear layer weights and biases in the neural field, for image generation. Henzler et al. [HMR20] learns 2D texture exemplars and maps them into 3D by sampling random noise fields at desired positions as the neural texture field input. PiCA [MSS*21] applies a lightweight SIREN to predict human facial texture over a guide mesh, where the 2D coordinate input lie in the UV space. Li et al. [LTW*21] use a 2D neural field to parameterize deformation, for recovering images distorted by turbulent refractive media.

Image Reconstruction: X-Fields [BMSR20] parameterizes the image as a 2D neural field conditioned on time and illumination to enable time and illumination interpolation. Alternatively, Nam et al. [NBB21] represents dynamic images (video) with 2D neural fields, with additional homography warp, optical flow, or occlusion operations to model dynamic changes. Kasten et al. [KOWD21] represent dynamic images as time-dependent 2D neural fields, where individual foreground components are segmented as atlas, and alpha composited to obtain the final rendering.

11. Robotics

Many robotics problems share similarities with visual computing, for instance 3D reconstruction to help robot navigation. Neural fields have recently been employed in robotics to great effect. Robotics requires complex perception systems that allow agents to efficiently infer, reason about, and manipulate such scene representations. In this section, we discuss neural fields for robot perception, planning, and control in detail.

11.1. Localization via Camera Parameter Estimation

Cameras observe the 3D world via 2D images. The projection of a world location onto the image plane is obtained through the extrinsic and intrinsic matrices, where the extrinsic matrix $[\mathbf{R}|\mathbf{t}]$ defines the 6DoF transformation between the world coordinate frame and the camera coordinate frame, while the intrinsics matrix \mathbf{K} describes the projection of a 3D point onto the 2D image plane. Commonly, these camera parameters are obtained via SFM and keypoint matching with off-the-shelf tools like COLMAP [SF16, SZPF16]. Since neural rendering is end-to-end differentiable, camera parameters can be jointly estimated with the neural field making them useful for Simultaneous Localization and Mapping (SLAM) [SLOD21] and Absolute Pose Regression (APR) [CWP21].

There exist numerous ways to parameterize camera matrices.

The pinhole camera model is a popular choice for the intrinsics matrix. Representing the extrinsics matrix, particularly rotation, however, is a long-standing challenge. Since the 3-by-3 rotation matrix lies on $SO(3)$, continuity is not guaranteed [ZBL*19, LEC*20]. Consequently, alternative parameterizations were used in neural field literature: exponential coordinates [YCFB*21], Rodriguez formula [WWX*21], continuous 6D representation [MCL*21, ZBL*19], Euler angle [AMBG*21], and homography warp (for planar scenes) [MCL*21, YCFB*21].

Furthermore, joint reconstruction and registration is a long-standing chicken-and-egg problem: camera parameters are needed to reconstruct the scene, and a reconstruction is needed to estimate camera parameters. One simplification is to assume known reconstruction and solve only the registration problem. iNeRF [YCFB*21] estimates camera poses given pre-trained neural fields, thus *inverting* the problem statement. Due to the strong assumption, iNeRF has a limited use case of registering new, un-posed images to an already-reconstructed scene. A coarse initialization of camera parameters alleviates the non-convex optimization problem. As such, several works *refine* camera parameters during reconstruction [AMBG*21, LMTL21, JAC*21, WWX*21, CWP21]. The chicken-and-egg nature of the problem is reflected by NeRF-[WWX*21], in which the authors jointly optimize the scene and cameras, but retrain scene reconstruction with the optimized camera parameters for better reconstruction quality.

The more challenging problem of estimating unknown camera parameters, while jointly reconstructing the scene has been looked into by several works [LMTL21, WWX*21]. However, the scene is assumed to be forward-facing and the camera pose initialization relies on hand-crafted rules (*e.g.*, cameras centered at origin, facing the $-z$ axis, with focal lengths equal to the reference image size [WWX*21]). GNeRF [MCL*21] further relaxes these assumptions, and supports inward-facing 360° scenes. The optimization between reconstruction and registration proceeds iteratively, rather than jointly, and are softly coupled via a discriminator. Approaches to overcome local minima in optimization and preserve details include coarse-to-fine training [LMTL21, JAC*21, CWP21], high-frequency positional encoding weights [CWP21, LMTL21], and curriculum learning [JAC*21] for optimizing focal lengths followed by intrinsics and lens distortion.

In the examples above, supervision is provided via appearance. Additional signals such as depth map from RGB-D sensor could provide strong signals for camera parameter optimization [SLOD21]. Similarly, time-of-flight image may also reduce the problem complexity [ALG*21]. A closely related topic is object pose estimation. While object pose can be modelled explicitly, a different approach is to predict a *probability distribution* of pose over $SO(3)$ [MEJ*21]. The probability distribution is itself a neural field, mapping rotation to probability. The approach is especially useful for symmetric objects with multiple valid solutions.

11.2. Planning

Planning in robotics is the problem of identifying a sequence of valid robot configuration states to achieve an objective. This includes path planning for navigation, trajectory planning for

grasping or manipulation, or planning for interactive perception [BHS*17]. Given the spatial nature of planning problems, neural fields have been used as a representation in many solutions.

Among the first attempts to use neural networks for robot path planning was by Lemmon [Lem91, Lem92]. While this work refers to a 2D grid of neurons as a “neural field,” the neurons are mapped one-to-one to a 2D map and is thus a (non-continuous) coordinate-based network. Their method finds the variational solution of Bellman’s dynamic programming equation [Bel54] used in path planning. Other coordinate-based representations have been used for planning, including estimating affordance maps [KS15, QMGR20]. Zhang et al. parameterize a Fisher Information Field [ZS20] via neural network. World constraints can be specified during planning, for example, by specifying constraints as a level set in a high-dimensional space [SFE*20] which is learned as a neural field.

Grasping and manipulation problems require knowing 2D or 3D position of a robot gripper relative to the surface of objects. Some approaches model the shape of the object as a collection of points [BKP11], and learn potentially good points for grasping or manipulation using a Markov Random Field (MRF). This approach can handle points in any continuous 3D position as long as an MRF can be built. Similarly, other data-driven grasping methods often use coordinate-based representations [BMAK14]. Contact-Nets [PHP20] models contact between objects via learned neural fields. Neural fields can also synthesize human grasps [KYZ*20]. GIGA [JZS*21] uses locally-conditioned neural fields encoding quality, orientation, width, and occupancy for grasp selection.

11.3. Control

Controllers are responsible for realizing plans, while ensuring that physical constraints and mechanical integrity are preserved. Control can be achieved either by relying on a planner or directly from observations. Neural fields have been used for this task by learning an obstacle barrier function approximated by an SDF [LQCA21]. Similarly, Bhardwaj et al. [BSM*21] solve the robot arm self-collision avoidance task by using neural fields to predict the closest distance between robot links, given its joint configuration. In visuomotor control, control is driven directly by visual observations. Li et al. [LLS*21] use NeRF to facilitate view-invariant visuomotor control to achieve robot goal states specified via a 2D goal image. This is achieved by auto-decoding a dynamics model to support future prediction and novel view synthesis.

12. Compression

The goal of lossy data compression is to approximate a signal with as few bits as possible. Signals are typically stored as discrete signals reparameterized with a transform such as the discrete cosine transform. Many standards exist, such as JPEG [Wal92] for images or HEVC [SOHW12] for videos. Recent work has explored the potential of neural fields as an alternate transform for lossy data compression. Compression may be achieved in one of two ways. First, by leveraging the inductive bias of the network architecture itself, and simply overfitting a neural field to a signal, *i.e.*, finding parameters Θ of a neural field Φ . Only the parameters and architecture of the neural field need to be stored. Second, *prior-based*

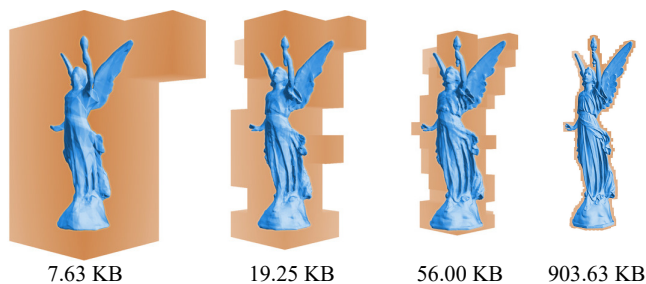


Figure 17: *Neural Level of Detail (NGLoD) combines level-of-detail with neural fields as a hybrid continuous-discrete shape representation, demonstrating compression of 3D geometry. Figure adapted from [TLY*21].*

compression schemes achieve compression via learning a space of low-dimensional latent code vectors \mathbf{z} that may be decoded into neural field parameters as discussed in Section 2, where the storage cost of the decoder is amortized over many latent codes.

Seminal work on encoding 3D geometry in neural fields [PFS*19, MON*19, CZ19] present an alternative to conventional mesh representations that may enable a significantly reduced memory footprint. Subsequently, SIREN [SMB*20] demonstrated fitting a wide array of signals with neural fields: audio, video, images, and 3D geometry (including large-scale scenes). Lu et al. [LJLB21] show that SIREN in conjunction with scalar weight quantization can compress dense volumetric data better than state-of-the-art approaches at the cost of higher encoding and decoding latency. Davies et al. [DNJ21] compare neural field 3D geometry with standard decimated meshes and found better reconstruction quality with the same memory footprint. Takikawa et al. [TLY*21] compare decimated meshes with a variable bitrate and level-of-detail representation (Figure 17). Dupont et al. [DGA*21] compared the memory use of neural fields parameterizing images, and found neural fields can outperform JPEG [Wal92] but not state-of-the-art image compression techniques. ACORN [MLL*21] use an adaptive quadtree data structure to fit high resolution images with neural fields, but do not outperform traditional image compression methods. For dynamic 3D scenes, DyNeRF [LSZ*21] uses 28 MB of memory for a 10-second 30 FPS 3D video sequence. Light Field Networks [SRF*21] compare the memory footprint of a neural field parameterizing a light field to the memory footprint of classical discrete light fields and find a drastic reduction in memory. General network compression and quantization techniques can further reduce network size [Isi21, BBSC21]. Bird et al. apply entropy penalization to NeRF [BBSC21], and obtain higher compression rates compared to standard HEVC video encoding [SOHW12] and LLFF [MSOC*19] for forward-facing scenes.

The above methods study a variety of continuous signals, but use different datasets, architectures, and metrics, making comparisons difficult. Few rigorous comparisons exist between neural field and conventional encoding schemes. Many works lack ablation of design choices and the ability to make direct queries to the without decoding. Neural fields for compression remains in its infancy.

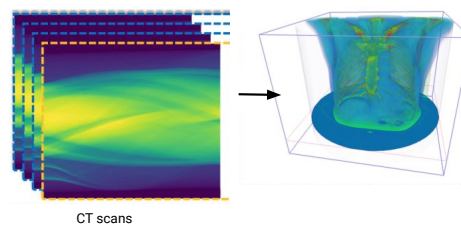


Figure 18: *Reconstruction of 3D density field (right) from limited-angle CT measurements (left). Figure adapted from [ZIL*21].*

13. Beyond Visual Computing

Visual computing problems are a subset of all inverse problems which can be parameterized by neural fields. These problems often share the same challenges involving incomplete observations and the need for a flexible parameterization. In this section we will highlight some of the emerging research directions beyond visual computing which may benefit from neural fields.

13.1. Alternative Imaging Modalities

Visual computing typically models and processes images from ‘off-the-shelf’ cameras: in the visible electromagnetic spectrum (light), formed through ray optics (lenses), and using sensors that exploit the photoelectric effect to digitize irradiance into intensity over a 2D raster grid (e.g. CCD or CMOS). Neural fields can also parameterize scenes captured under alternative imaging modalities such as non-line-of-sight imaging [SWL*21], non-visible x-rays for computed tomography (CT) [SPX21, ZIL*21, SLX*21], and non EM imaging like magnetic resonance imaging (MRI) [SPX21], pressure waves for audio [RBBJ], chemiluminescence [PXZ*21] or time-of-flight images [ALG*21]. Volumetric light displays use a spatially-varying physical absorbing medium and light source to attenuate light into image. The absorption coefficient can be modelled by neural fields [ZBW*20].

13.2. Medical Imaging via CT and MRI

In CT and MRI, raw sensor measurements are the Radon and Fourier transformation of spatially-varying density, respectively [SPX21]. The sensor domains are not human-readable, while the reconstructed density volume (whose 2D slices are called the image domain) is. Reconstructing the density volume is an ill-posed problem [SPX21], and classical techniques are sensitive to measurement noise [ZIL*21]. Reconstruction and NVS in medical imaging is also limited by capture constraints such as scene movement, finite sensor resolution, limited viewing angle, and sparse views (to reduce X-ray exposure, and speed up procedure).

Neural fields can either parameterize the sensor domain [SLX*21], or the density domain directly [SPX21, ZIL*21]. In the former, the neural field maps sensor coordinates to predicted sensor activations, and can augment real measurement data, before applying classical reconstruction technique (filtered back-projection [KS01]) [SLX*21]. In the latter the neural field directly predicts the density value at a 3D spatial coordinate, and is supervised by mapping its output to the sensor domain via Radon (CT) or Fourier (MRI) transform [SPX21, ZIL*21].

Similarly, in cryo-electron microscopy (cryo-EM), the 2D sensor measures the convolution between a point spread function and electron density. In CryoGRGN [ZBDB20b], the neural field maps a 3D coordinate to the deconvolved electron density.

13.3. Audio

Audio signals can be represented as raw waveforms or spectrograms, and each can be parameterized by neural fields [SMB*20, GCM*21]. Raw waveform is a continuous 1D field function that maps temporal coordinates to amplitude, often stored as a collection of discrete samples. A spectrogram is the Fourier transform of a waveform, which is a 2D field function mapping time and frequency to amplitude. Neural field methods fit all time-dependent waveforms, which means that the techniques are applicable to all waves mechanical (e.g., seismic waves, ocean waves, acoustic waves) or electromagnetic (e.g., wave optics, radio waves).

Synthetic aperture sonar (SAS) also exhibits the common problems in inverse problems: noisy sensor domain and ill-posed problem. Reed et al. [RBBJ] use a neural field mapping a 2D position to a distribution of point scatter (reconstruction domain), and obtain supervision by mapping to the sensor domain via convolution.

13.4. Physics-informed Problems

Physics-informed problems have solutions that are restricted to a set of partial differential equations (PDEs) based on laws of physics. The solutions are often continuous in spatio-temporal coordinates. Neural fields are therefore a natural parameterization of the solution space, given that neural networks are continuous, differentiable, and universal function approximators. These neural fields are also referred to as physics-informed neural networks (PINNs), whose use was first popularized by [RPK19]. Problems constrained by nonlinear PDEs often require arbitrarily-small step sizes for traditional methods, which often require prohibitive computation resources. Parameterizing the solution via neural networks re-formulates these problems as *optimization*, rather than *simulation*, which is more data-efficient [RPK19]. Since many physical processes in nature are governed by PDEs (boundary conditions), supervising (or regularizing) the neural network via its gradients is a common technique. In fact, the Eikonal regularization for SDF is an example in visual computing. Physics-informed problems include topology optimization [ZLCT21], geodesy estimation [IG21], collision dynamics estimation [PHP20], solving the Schrodinger Equation [RPK19], Navier-Stokes equation [RPK19], and Eikonal equation [SAR20].

Discussion & Conclusion

14. Discussion

As we have seen, neural fields have a rich but evolving technical ‘toolbox’, and a rapidly increasing space of applications both within and outside of visual computing. In our view, there are several factors that have resulted in this progress. First, the idea of continuously parameterizing a *field* using an MLP without the need to use more complex neural network architectures has simplified the training of fields and reduced the entry barrier [GN98].

Neural fields provide a fundamentally different view of signal processing that is no longer discrete but rather faithful to the original *continuous* signal. Second, techniques such as positional encoding and sinusoidal activations have significantly improved the quality of neural fields leading to large leaps in applications focused on quality. Finally, applications in novel view synthesis and 3D reconstruction have been particularly important in popularizing neural fields because of the visually appealing nature of these applications [GFK*18b, PFS*19, MST*20, SZW19].

Future Directions: Despite the progress, we believe that neural fields have only started to scratch the surface and there remains great potential for continued progress in both techniques and methods. Thus far, neural fields have primarily been used to solve “low-level” (e.g., image synthesis) and “mid-level” (e.g., 3D reconstruction) tasks. We believe that “high-level” tasks that involve grouping of data into more meaningful concepts is a fruitful direction of future work [TLV21]. A common limitation of many neural fields is their inability to generalize well to new data. We believe that integration of stronger priors can enable these methods to generalize better and be data efficient. Other inductive biases in the form of the laws of physics, or network architecture can further help generalization. Furthermore, the rapid progress has been at the expense of methodical evaluation and analysis of techniques which we think should be addressed in the future. Finally, we believe that the community must pay more careful attention to past work to avoid “*selective amnesia*” [SC21] and repetition of work.

Societal Impact: As the applications of neural fields increase, so will their societal impact, especially in domains where they make a significant difference. In generative modeling of audio, imagery, 3D scenes, etc., neural fields have enabled the generation of realistic content for the purpose of deception, for instance, impersonating the image and voice of actors without their consent. A large amount of recent work explores the detection of such digitally altered imagery [TVRF*20]. Similarly, improving the capabilities of inverse-problem solvers, such as denoising and blur-removal algorithms, has significant implications for privacy. For instance, this may enable de-anonymizing recordings that were previously assumed to not contain sufficient information to allow identification of participating actors. It may also decrease the cost of surveillance, making it more widely available, as the hardware requirements may decrease. Finally, neural fields could also have negative environmental impact as significant computational resources are spent optimizing neural networks with GPUs.

Neural fields can also positively impact society. Democratizing the generation of photo-realistic imagery helps artists and content creators to tell their stories better. The ability to aggregate information from low-dimensional supervision (e.g., 2D images) relaxes the hardware constraint for 3D content creation. Neural fields for computer vision can become key enablers of a future where automation helps people.

15. Conclusion

This report provides an overview of the flourishing research direction of neural fields. From a review of 251 papers, we have summarized five classes of techniques using a shared mathematical formulation, including generalization, hybrid representations, forward

maps, network architectures, and manipulation methods. Then, we have surveyed applications across graphics, vision, robotics, medical imaging, and computational physics. Neural fields research will continue to grow. To aid in continued understanding, we have established a living report as a [community-driven website](#), where authors can submit their own papers and classify them using the taxonomy developed in this report. Neural fields will be a key enabler for progress across many areas of computer science, and we look forward to the research yet to come.

Authors

Yiheng Xie (<https://yxie20.github.io/>) is a final-year undergraduate student at Brown University and a researcher at Unity Technologies. His research interests include 3D reconstruction, physically-based rendering, and robotics. He is a member of Brown Visual Computing (BVC), advised by Professor Srinath Sridhar, and Brown Humanity Centered Robotics Initiative (HCRI), advised by Professor Michael Littman.

Towaki Takikawa (<https://tovacinni.github.io/>) is a Ph.D. student at the University of Toronto with Prof. Sanja Fidler and Prof. Alec Jacobson. He is also a Research Scientist at NVIDIA in the Hyperscale Graphics Systems group. He received his bachelors in Computer Science at the University of Waterloo.

Shunsuke Saito (<http://www-scf.usc.edu/~saitos/>) is a Research Scientist at Reality Labs Research in Pittsburgh. He finished his Ph.D. at University of Southern California, where he worked with Prof. Hao Li. Prior to USC, he spent one year at University of Pennsylvania as Visiting Researcher. He obtained B.Eng. and M.Eng. in Applied Physics at Waseda University in 2013 and 2014.

Or Litany (<https://orlitany.github.io/>) is a Research Scientist at NVIDIA. Prior, he was a postdoc at Stanford University working under Prof. Leonidas Guibas, and a postdoc at FAIR working under Prof. Jitendra Malik. Previously, he was a postdoc at the Technion and a research intern at Microsoft, Intel and Google. He received his PhD from Tel-Aviv University, advised by Prof. Alex Bronstein. He received my B.Sc. in Physics and Mathematics from the Hebrew University under the auspices of “Talpiot.”

Shiqin Yan (<https://player-eric.com/about>) is a masters student in Computer Science at Brown University. He is passionate about solving real-world problems with large-scale web-based systems.

Numair Khan (<http://cs.brown.edu/~nkhan6/>) is a PhD student at Brown University where his research focuses on methods and representations for scene reconstruction, differentiable rendering, and novel-view synthesis.

Federico Tombari (<https://federicotombari.github.io/>) is a Research Scientist and Manager at Google Zurich (Switzerland), where he leads an applied research team in Computer Vision and Machine Learning. He is also affiliated to the Faculty of Computer Science at TU Munich (Germany) as lecturer (Privatdozent).

James Tompkin (<https://jamestompkin.com/>) is an assistant professor in visual computing at Brown University. He was a PhD student at UCL, with postdocs at the Max Planck Institute and Harvard. His lab develops visual understanding techniques for camera-captured media to remove barriers from image and video creation, editing, and interaction. This requires image and scene reconstruction techniques, especially from multi-camera systems.

Vincent Sitzmann (<https://vsitzmann.github.io/>) is an incoming assistant professor at MIT EECS. Currently, he is a Postdoc at MIT’s CSAIL with Joshua Tenenbaum, William Freeman, and Frédo Durand. Previously, he finished his Ph.D. at Stanford University. His research interest lies in neural scene representations — the way neural networks learn to represent information on our world. His goal is to allow independent agents to reason about our world given visual observations, such as inferring a complete model of

a scene with information on geometry, material, lighting etc. from only few observations, a task that is simple for humans, but currently impossible for AI.

Srinath Sridhar (<https://srinathsriddhar.com/>) is an assistant professor of computer science at Brown University. His research interests are in 3D computer vision and machine learning. Specifically, he focuses on visual understanding of 3D human physical interactions with applications ranging from robotics to mixed reality. He has won several fellowships (e.g., Google Research Scholar) and awards (e.g., Eurographics Best Paper Honorable Mention) for his work, and has previously spent time at Stanford, Max Planck Institute for Informatics, Microsoft Research Redmond, and Honda Research Institute.

Acknowledgements

This work was supported by an NSF grant (CNS-2038897) and the Google Research Scholar Program. We would like to thank Sunny Li for their help in designing the website, and Alexander Rush and Hendrik Strobel of the [Mini-Conf](#) project.

References

- [ADK*21] ANOKHIN I., DEMOCHKIN K., KHAKHULIN T., STERKIN G., LEMPITSKY V., KORZHENKOV D.: Image generators with conditionally-independent pixel synthesis. In *Proceedings of the IEEE/CVF Conference on Computer Vision and Pattern Recognition (CVPR)* (2021). URL: <http://arxiv.org/abs/2011.13775v1>. 16, 17
- [AHY*19] ATZMON M., HAIM N., YARIV L., ISRAELOV O., MARON H., LIPMAN Y.: Controlling neural level sets. In *Advances in Neural Information Processing Systems (NeurIPS)* (2019), Curran Associates, Inc. URL: <http://arxiv.org/abs/1905.11911v2>. 12
- [AL20a] ATZMON M., LIPMAN Y.: Sal: Sign agnostic learning of shapes from raw data. In *Proceedings of the IEEE/CVF Conference on Computer Vision and Pattern Recognition (CVPR)* (2020). URL: <http://arxiv.org/abs/1911.10414v2>. 12
- [AL20b] ATZMON M., LIPMAN Y.: Sald: Sign agnostic learning with derivatives. *arXiv preprint arXiv:2006.05400* (2020). 13
- [ALG*21] ATTAL B., LAIDLAW E., GOKASLAN A., KIM C., RICHARDT C., TOMPKIN J., O'TOOLE M.: Torf: Time-of-flight radiance fields for dynamic scene view synthesis. In *Advances in Neural Information Processing Systems (NeurIPS)* (2021), Curran Associates, Inc. URL: <http://arxiv.org/abs/2109.15271v1>. 15, 18, 19
- [AMBG*21] AZINOVIC D., MARTIN-BRUALLA R., GOLDMAN D. B., NIESSNER M., THIES J.: Neural rgb-d surface reconstruction. *arXiv preprint arXiv:2104.04532* (2021). URL: <http://arxiv.org/abs/2104.04532v1>. 18
- [Ano22] ANONYMOUS: Stylerf: A style-based 3d aware generator for high-resolution image synthesis. In *Submitted to The Tenth International Conference on Learning Representations* (2022). URL: <https://openreview.net/forum?id=iUuzzTMUw9K>. 17
- [ANVL21] ATZMON M., NOVOTNY D., VEDALDI A., LIPMAN Y.: Augmenting implicit neural shape representations with explicit deformation fields. *arXiv preprint arXiv:2108.08931* (2021). URL: <http://arxiv.org/abs/2108.08931v1>. 10
- [ASS21] ATHAR S., SHU Z., SAMARAS D.: Flame-in-nerf: Neural control of radiance fields for free view face animation. *arXiv preprint arXiv:2108.04913* (2021). URL: <http://arxiv.org/abs/2108.04913v1>. 10, 12, 15
- [AXS21] ALLDIECK T., XU H., SMINCHISESCU C.: imghum: Implicit generative models of 3d human shape and articulated pose. In *Proceedings of the IEEE/CVF Conference on Computer Vision and Pattern Recognition (CVPR)* (2021). URL: <http://arxiv.org/abs/2108.10842v1>. 16
- [AZ21] ARANDJELOVIĆ R., ZISSERMAN A.: Nerf in detail: Learning to sample for view synthesis. *arXiv preprint arXiv:2106.05264* (2021). 13
- [BBJ*21] BOSS M., BRAUN R., JAMPANI V., BARRON J. T., LIU C., LENSCH H. P. A.: Nerd: Neural reflectance decomposition from image collections. In *Proceedings of the IEEE International Conference on Computer Vision (ICCV)* (2021). URL: <http://arxiv.org/abs/2012.03918v4>. 14
- [BBSC21] BIRD T., BALLE J., SINGH S., CHOU P. A.: 3d scene compression through entropy penalized neural representation functions. *arXiv preprint arXiv:2104.12456* (2021). URL: <http://arxiv.org/abs/2104.12456v1>. 19
- [Bel54] BELLMAN R.: The theory of dynamic programming. *Bulletin of the American Mathematical Society* 60, 6 (1954), 503–515. 18
- [BHS*17] BOHG J., HAUSMAN K., SANKARAN B., BROCK O., KRAGIC D., SCHAAL S., SUKHATME G. S.: Interactive perception: Leveraging action in perception and perception in action. *IEEE Transactions on Robotics* 33, 6 (2017), 1273–1291. doi:10.1109/TRO.2017.2721939. 18
- [BHumRZ21] BENBARKA N., HOFER T., UL-MOQEET RIAZ H., ZELL A.: Seeing implicit neural representations as fourier series. *arXiv preprint arXiv:2109.00249* (2021). URL: <http://arxiv.org/abs/2109.00249v1>. 9
- [BJLPS17] BOJANOWSKI P., JOULIN A., LOPEZ-PAZ D., SZLAM A.: Optimizing the latent space of generative networks. *arXiv preprint arXiv:1707.05776* (2017). 16
- [BKP11] BOULARIAS A., KROEMER O., PETERS J.: Learning robot grasping from 3-d images with markov random fields. In *2011 IEEE/RSJ International Conference on Intelligent Robots and Systems* (2011), pp. 1548–1553. doi:10.1109/IROS.2011.6094888. 18
- [BMAK14] BOHG J., MORALES A., ASFOUR T., KRAGIC D.: Data-driven grasp synthesis—a survey. *IEEE Transactions on Robotics* 30, 2 (2014), 289–309. doi:10.1109/TRO.2013.2289018. 18
- [BMSR20] BEMANA M., MYSZKOWSKI K., SEIDEL H.-P., RITSCHEL T.: X-fields: Implicit neural view-, light- and time-image interpolation. *ACM Transactions on Graphics (TOG)* (2020). URL: <http://arxiv.org/abs/2010.00450v1>. 10, 12, 17
- [BMT*21] BARRON J. T., MILDENHALL B., TANCIK M., HEDMAN P., MARTIN-BRUALLA R., SRINIVASAN P. P.: Mip-nerf: A multiscale representation for anti-aliasing neural radiance fields. In *Proceedings of the IEEE International Conference on Computer Vision (ICCV)* (2021). URL: <http://arxiv.org/abs/2103.13415v3>. 13
- [BPRS18] BAYDIN A. G., PEARLMUTTER B. A., RADUL A. A., SISKIND J. M.: Automatic differentiation in machine learning: a survey. *Journal of machine learning research* 18 (2018). 10
- [BS12] BURLEY B., STUDIOS W. D. A.: Physically-based shading at disney. In *ACM SIGGRAPH* (2012), vol. 2012, pp. 1–7. 8, 14
- [BSM*21] BHARDWAJ M., SUNDARALINGAM B., MOUSAVIAN A., RATLIFF N., FOX D., RAMOS F., BOOTS B.: Fast joint space model-predictive control for reactive manipulation. *arXiv preprint arXiv:2104.13542* (2021). 18
- [BSTPM20a] BHATNAGAR B. L., SMINCHISESCU C., THEOBALT C., PONS-MOLL G.: Combining implicit function learning and parametric models for 3d human reconstruction. In *Proceedings of the European Conference on Computer Vision (ECCV)* (2020). URL: <http://arxiv.org/abs/2007.11432v1>. 15, 16
- [BSTPM20b] BHATNAGAR B. L., SMINCHISESCU C., THEOBALT C., PONS-MOLL G.: Loopreg: Self-supervised learning of implicit surface correspondences, pose and shape for 3d human mesh registration. In *Advances in Neural Information Processing Systems (NeurIPS)*

- (2020), Curran Associates, Inc. URL: <http://arxiv.org/abs/2010.12447v1>. 16
- [BTW21] BOND-TAYLOR S., WILLCOCKS C. G.: Gradient origin networks. *Proc. ICLR* (2021). 16
- [BV99] BLANZ V., VETTER T.: A morphable model for the synthesis of 3d faces. In *Proceedings of the 26th annual conference on Computer graphics and interactive techniques* (1999), pp. 187–194. 15
- [BXS*20] BI S., XU Z., SRINIVASAN P., MILDENHALL B., SUNKAVALLI K., HASAN M., HOLD-GEOFFROY Y., KRIEGMAN D., RAMAMOORTHY R.: Neural reflectance fields for appearance acquisition. *arXiv preprint arXiv:2008.03824* (2020). URL: <http://arxiv.org/abs/2008.03824v2>. 14
- [CAMNS21] CHATZIAGAPI A., ATHAR S., MORENO-NOGUER F., SAMARAS D.: Sider: Single-image neural optimization for facial geometric detail recovery. *arXiv preprint arXiv:2108.05465* (2021). URL: <http://arxiv.org/abs/2108.05465v1>. 15
- [CAPM20] CHIBANE J., ALLDIECK T., PONS-MOLL G.: Implicit functions in feature space for 3d shape reconstruction and completion. In *Proceedings of the IEEE/CVF Conference on Computer Vision and Pattern Recognition (CVPR)* (2020). URL: <http://arxiv.org/abs/2003.01456v2>. 5, 12, 15
- [CbGPW14] COOMBS S., BEIM GRABEN P., POTTHAST R., WRIGHT J.: *Neural fields: theory and applications*. Springer, 2014. 3
- [CBLPM21] CHIBANE J., BANSAL A., LAZOVA V., PONS-MOLL G.: Stereo radiance fields (srf): Learning view synthesis for sparse views of novel scenes. In *Proceedings of the IEEE/CVF Conference on Computer Vision and Pattern Recognition (CVPR)* (2021). URL: <http://arxiv.org/abs/2104.06935v1>. 13
- [CCA*21] CZERKAWSKI M., CARDONA J., ATKINSON R., MICHIE C., ANDONOVIC I., CLEMENTE C., TACHTATZIS C.: Neural knits: Patched neural implicit representation networks. *arXiv preprint arXiv:2109.14406* (2021). URL: <http://arxiv.org/abs/2109.14406v1>. 17
- [CFG*15] CHANG A. X., FUNKHOUSER T., GUIBAS L., HANRAHAN P., HUANG Q., LI Z., SAVARESE S., SAVVA M., SONG S., SU H., XIAO J., YI L., YU F.: *ShapeNet: An Information-Rich 3D Model Repository*. Tech. Rep. arXiv:1512.03012 [cs.GR], Stanford University — Princeton University — Toyota Technological Institute at Chicago, 2015. 12
- [Cha13] CHANDRASEKHAR S.: *Radiative transfer*. Courier Corporation, 2013. 8
- [CLCO*21] CHEN X., LI W., COHEN-OR D., MITRA N. J., CHEN B.: Moco-flow: Neural motion consensus flow for dynamic humans in stationary monocular cameras. *arXiv preprint arXiv:2106.04477* (2021). URL: <http://arxiv.org/abs/2106.04477v1>. 10
- [CLI*20] CHABRA R., LENSSEN J. E., ILG E., SCHMIDT T., STRAUB J., LOVEGROVE S., NEWCOMBE R.: Deep local shapes: Learning local sdf priors for detailed 3d reconstruction. In *Proceedings of the European Conference on Computer Vision (ECCV)* (2020). URL: <http://arxiv.org/abs/2003.10983v3>. 5, 7, 12
- [CLW21] CHEN Y., LIU S., WANG X.: Learning continuous image representation with local implicit image function. In *Proceedings of the IEEE/CVF Conference on Computer Vision and Pattern Recognition (CVPR)* (2021). URL: <http://arxiv.org/abs/2012.09161v2>. 17
- [CMK*21] CHAN E. R., MONTEIRO M., KELLNHOFER P., WU J., WETZSTEIN G.: pi-gan: Periodic implicit generative adversarial networks for 3d-aware image synthesis. In *Proceedings of the IEEE/CVF Conference on Computer Vision and Pattern Recognition (CVPR)* (2021). URL: <http://arxiv.org/abs/2012.00926v2>. 6, 7, 16
- [CPA*21] CORONA E., PUMAROLA A., ALENYA G., PONS-MOLL G., MORENO-NOGUER F.: Smplicit: Topology-aware generative model for clothed people. In *Proceedings of the IEEE/CVF Conference on Computer Vision and Pattern Recognition (CVPR)* (2021). URL: <http://arxiv.org/abs/2103.06871v2>. 16
- [CT82] COOK R. L., TORRANCE K. E.: A reflectance model for computer graphics. *ACM Transactions on Graphics (ToG)* 1, 1 (1982), 7–24. 8, 14
- [CTT*21] CHIANG P.-Z., TSAI M.-S., TSENG H.-Y., SHENG LAI W., CHIU W.-C.: Stylizing 3d scene via implicit representation and hypernetwork/meta-learning. *arXiv preprint arXiv:2105.13016* (2021). URL: <http://arxiv.org/abs/2105.13016v2>. 5, 11, 12
- [CWP21] CHEN S., WANG Z., PRISACARIU V.: Direct-posenet: Absolute pose regression with photometric consistency. *arXiv preprint arXiv:2104.04073* (2021). URL: <http://arxiv.org/abs/2104.04073v1>. 17, 18
- [CXZ*21] CHEN A., XU Z., ZHAO F., ZHANG X., XIANG F., YU J., SU H.: Mvsnrf: Fast generalizable radiance field reconstruction from multi-view stereo. In *Proceedings of the IEEE International Conference on Computer Vision (ICCV)* (2021). URL: <http://arxiv.org/abs/2103.15595v2>. 13
- [CZ19] CHEN Z., ZHANG H.: Learning implicit fields for generative shape modeling. In *Proceedings of the IEEE/CVF Conference on Computer Vision and Pattern Recognition (CVPR)* (2019). URL: <http://arxiv.org/abs/1812.02822v5>. 2, 11, 12, 16, 19
- [CZB*21] CHEN X., ZHENG Y., BLACK M. J., HILLIGES O., GEIGER A.: Snarf: Differentiable forward skinning for animating non-rigid neural implicit shapes. In *Proceedings of the IEEE International Conference on Computer Vision (ICCV)* (2021). URL: <http://arxiv.org/abs/2104.03953v1>. 10, 11, 16
- [CZK*21] CHEN J., ZHANG Y., KANG D., ZHE X., BAO L., JIA X., LU H.: Animatable neural radiance fields from monocular rgb videos. In *Proceedings of the IEEE International Conference on Computer Vision (ICCV)* (2021). URL: <http://arxiv.org/abs/2106.13629v2>. 16
- [DBS*21] DEVRIES T., BAUTISTA M. A., SRIVASTAVA N., TAYLOR G. W., SUSSKIND J. M.: Unconstrained scene generation with locally conditioned radiance fields. In *Proceedings of the IEEE International Conference on Computer Vision (ICCV)* (2021). URL: <http://arxiv.org/abs/2104.00670v1>. 5
- [DCTS21] DU Y., COLLINS M. K., TENENBAUM B. J., SITZMANN V.: Learning signal-agnostic manifolds of neural fields. In *Proc. NeurIPS* (2021). 17
- [DGA*21] DUPONT E., GOLINSKI A., ALIZADEH M., TEH Y. W., DOUCET A.: Coin: Compression with implicit neural representations. In *International Conference on Learning Representations* (2021). URL: <http://arxiv.org/abs/2103.03123v2>. 19
- [DGP*19] DEPRELLE T., GROUEIX T., FISHER M., KIM V. G., RUSSELL B. C., AUBRY M.: Learning elementary structures for 3d shape generation and matching. In *Proceedings of the IEEE International Conference on Computer Vision (ICCV)* (2019). URL: <http://arxiv.org/abs/1908.04725v2>. 12
- [DGY*20] DENG B., GENOVA K., YAZDANI S., BOUAZIZ S., HINTON G., TAGLIASACCHI A.: Cvxnet: Learnable convex decomposition. In *Proc. CVPR* (2020), pp. 31–44. 12
- [DLJ*20] DENG B., LEWIS J., JERUZALSKI T., PONS-MOLL G., HINTON G., NOROUZI M., TAGLIASACCHI A.: Nasa: Neural articulated shape approximation. In *Proceedings of the European Conference on Computer Vision (ECCV)* (2020). URL: <http://arxiv.org/abs/1912.03207v4>. 2, 11, 16
- [DNJ21] DAVIES T., NOWROUZSAHRAI D., JACOBSON A.: On the effectiveness of weight-encoded neural implicit 3d shapes. In *International Conference on Machine Learning (ICML)* (2021), PMLR. URL: <http://arxiv.org/abs/2009.09808v3>. 19
- [DPS*18] DUMOULIN V., PEREZ E., SCHUCHER N., STRUB F., DE VRIES H., COURVILLE A., BENGIO Y.: Feature-wise transformations. *Distill* 3, 7 (2018), e11. 5, 6
- [DVPL21] DEHESA J., VIDLER A., PADGET J., LUTTEROTH C.: Grid-functioned neural networks. In *Proceedings of the 38th International*

- Conference on Machine Learning (18–24 Jul 2021), Meila M., Zhang T., (Eds.), vol. 139 of *Proceedings of Machine Learning Research*, PMLR, pp. 2559–2567. URL: <https://proceedings.mlr.press/v139/dehesa21a.html>. 7
- [DW85] DIPPÉ M. A., WOLD E. H.: Antialiasing through stochastic sampling. In *Proceedings of the 12th annual conference on Computer graphics and interactive techniques* (1985), pp. 69–78. 8
- [DZY*21] DU Y., ZHANG Y., YU H.-X., TENENBAUM J. B., WU J.: Neural radiance flow for 4d view synthesis and video processing. In *Proceedings of the IEEE International Conference on Computer Vision (ICCV)* (2021). URL: <http://arxiv.org/abs/2012.09790v2>. 11, 15
- [Eva15] EVANS A.: Learning from failure: a survey of promising, unconventional and mostly abandoned renderers for ‘dreams ps4’, a geometrically dense, painterly ugc game. *Advances in Real-Time Rendering in Games. MediaMolecule, SIGGRAPH* (2015). 2
- [FAL17] FINN C., ABBEEL P., LEVINE S.: Model-agnostic meta-learning for fast adaptation of deep networks. In *International Conference on Machine Learning* (2017), PMLR, pp. 1126–1135. 6
- [FC19] FRANKLE J., CARBIN M.: The lottery ticket hypothesis: Finding sparse, trainable neural networks. *Proc. ICLR* (2019). 3
- [Flo03] FLOATER M. S.: Mean value coordinates. *Computer aided geometric design* 20, 1 (2003), 19–27. 7
- [FLS65] FEYNMAN R. P., LEIGHTON R. B., SANDS M.: The feynman lectures on physics; vol. i. *American Journal of Physics* 33, 9 (1965), 750–752. 2
- [FSSV07] FLÓREZ J., SBERT M., SAINZ M. A., VEHÍ J.: Efficient ray tracing using interval analysis. In *International Conference on Parallel Processing and Applied Mathematics* (2007), Springer, pp. 1351–1360. 8
- [G*89] GRIEWANK A., ET AL.: On automatic differentiation. *Mathematical Programming: recent developments and applications* 6, 6 (1989), 83–107. 10
- [GCL*21] GUO Y., CHEN K., LIANG S., LIU Y.-J., BAO H., ZHANG J.: Ad-nerf: Audio driven neural radiance fields for talking head synthesis. In *Proceedings of the IEEE International Conference on Computer Vision (ICCV)* (2021). URL: <http://arxiv.org/abs/2103.11078v3>. 4
- [GCM*21] GAO R., CHANG Y.-Y., MALL S., FEI-FEI L., WU J.: Objectfolder: A dataset of objects with implicit visual, auditory, and tactile representations. In *Proceedings of the Conference on Robot Learning (CoRL)* (2021). URL: <http://arxiv.org/abs/2109.07991v2>. 8, 20
- [GCS*20] GENOVA K., COLE F., SUD A., SARNA A., FUNKHOUSER T.: Local deep implicit functions for 3d shape. In *Proceedings of the IEEE/CVF Conference on Computer Vision and Pattern Recognition (CVPR)* (2020). URL: <http://arxiv.org/abs/1912.06126v2>. 11, 12
- [GFK*18a] GROUEIX T., FISHER M., KIM V. G., RUSSELL B. C., AUBRY M.: 3d-coded : 3d correspondences by deep deformation, 2018. [arXiv:1806.05228](https://arxiv.org/abs/1806.05228). 16
- [GFK*18b] GROUEIX T., FISHER M., KIM V. G., RUSSELL B. C., AUBRY M.: Atlasnet: A papier-mache approach to learning 3d surface generation. In *Proceedings of the IEEE/CVF Conference on Computer Vision and Pattern Recognition (CVPR)* (2018). URL: <http://arxiv.org/abs/1802.05384v3>. 6, 12, 20
- [GFWF20] GUO M., FATHI A., WU J., FUNKHOUSER T.: Object-centric neural scene rendering. *arXiv preprint arXiv:2012.08503* (2020). URL: <http://arxiv.org/abs/2012.08503v1>. 7
- [GGPP20] GALIN E., GUÉRIN E., PARIS A., PEYTAVIE A.: Segment tracing using local lipschitz bounds. In *Computer Graphics Forum* (2020), vol. 39, Wiley Online Library, pp. 545–554. 8
- [GKJ*21] GARBIN S. J., KOWALSKI M., JOHNSON M., SHOTTON J., VALENTIN J.: Fastnerf: High-fidelity neural rendering at 200fps. *arXiv preprint arXiv:2103.10380* (2021). URL: <http://arxiv.org/abs/2103.10380v2>. 13
- [GN98] GARGAN D., NEELAMKAVIL F.: Approximating reflectance functions using neural networks. *Computer Graphics Forum* (1998), 23–34. 8, 20
- [Gre86] GREENE N.: Environment mapping and other applications of world projections. *IEEE computer graphics and Applications* 6, 11 (1986), 21–29. 8
- [Gre03] GREEN R.: Spherical harmonic lighting: The gritty details. In *Archives of the game developers conference* (2003), vol. 56, p. 4. 8
- [GSKH21] GAO C., SARAF A., KOPF J., HUANG J.-B.: Dynamic view synthesis from dynamic monocular video. *arXiv preprint arXiv:2105.06468* (2021). URL: <http://arxiv.org/abs/2105.06468v1>. 10, 11, 15
- [GSL*20] GAO C., SHIH Y., LAI W.-S., LIANG C.-K., HUANG J.-B.: Portrait neural radiance fields from a single image. *arXiv preprint arXiv:2012.05903* (2020). URL: <http://arxiv.org/abs/2012.05903v2>. 5, 15
- [GSRN21] GRANSKOG J., SCHNABEL T. N., ROUSSELLE F., NOVÁK J.: Neural scene graph rendering. *ACM Transactions on Graphics (TOG)* 40, 4 (2021), 1–11. 7
- [GTZN21] GAFNI G., THIES J., ZOLLHOFFER M., NIESSNER M.: Dynamic neural radiance fields for monocular 4d facial avatar reconstruction. In *Proceedings of the IEEE/CVF Conference on Computer Vision and Pattern Recognition (CVPR)* (2021). URL: <http://arxiv.org/abs/2012.03065v1>. 12, 15
- [GW20] GALANTI T., WOLF L.: On the modularity of hypernetworks. *Proc. NeurIPS* (2020). 5
- [GYH*20] GROPP A., YARIV L., HAIM N., ATZMON M., LIPMAN Y.: Implicit geometric regularization for learning shapes. In *Proceedings of the IEEE/CVF Conference on Computer Vision and Pattern Recognition (CVPR)* (2020). URL: <http://arxiv.org/abs/2002.10099v2>. 9, 12
- [HAESB20] HAO Z., AVERBUCH-ELOR H., SNAVELY N., BELONGIE S.: Dualsdf: Semantic shape manipulation using a two-level representation. In *Proceedings of the IEEE/CVF Conference on Computer Vision and Pattern Recognition (CVPR)* (2020). URL: <http://arxiv.org/abs/2004.02869v1>. 11, 12
- [Har96] HART J. C.: Sphere tracing: A geometric method for the antialiased ray tracing of implicit surfaces. *The Visual Computer* 12, 10 (1996), 527–545. 8
- [HCJS20] HE T., COLLOMOSSE J., JIN H., SOATTO S.: Geo-pifu: Geometry and pixel aligned implicit functions for single-view human reconstruction. In *Advances in Neural Information Processing Systems (NeurIPS)* (2020), Curran Associates, Inc. URL: <http://arxiv.org/abs/2006.08072v2>. 15
- [HDL16] HA D., DAI A., LE Q.: Hypernetworks. In *International Conference on Learning Representations* (2016). 5
- [HIL*20] HALIMI O., IMANUEL I., LITANY O., TRAPPOLINI G., RODOLÀ E., GUIBAS L., KIMMEL R.: The whole is greater than the sum of its nonrigid parts, 2020. [arXiv:2001.09650](https://arxiv.org/abs/2001.09650). 16
- [HJKK21] HU Z., JAGTAP A. D., KARNIADAKIS G. E., KAWAGUCHI K.: When do extended physics-informed neural networks (xpinn) improve generalization? *arXiv preprint arXiv:2109.09444* (2021). URL: <http://arxiv.org/abs/2109.09444v2>. 7
- [HMBL21] HAO Z., MALLYA A., BELONGIE S., LIU M.-Y.: Gancraft: Unsupervised 3d neural rendering of minecraft worlds. In *Proceedings of the IEEE International Conference on Computer Vision (ICCV)* (2021). URL: <http://arxiv.org/abs/2104.07659v1>. 7
- [HMR20] HENZLER P., MITRA N. J., RITSCHER T.: Learning a neural 3d texture space from 2d exemplars. In *Proceedings of the*

- IEEE/CVF Conference on Computer Vision and Pattern Recognition (CVPR)* (2020). URL: <http://arxiv.org/abs/1912.04158v2>. 17
- [HPG*21] HERTZ A., PEREL O., GIRYES R., SORKINE-HORNUNG O., COHEN-OR D.: Sape: Spatially-adaptive progressive encoding for neural optimization. *arXiv preprint arXiv:2104.09125* (2021). URL: <http://arxiv.org/abs/2104.09125v2>. 9
- [HSM*21] HEDMAN P., SRINIVASAN P. P., MILDENHALL B., BARRON J. T., DEBEVEC P.: Baking neural radiance fields for real-time view synthesis. *arXiv preprint arXiv:2103.14645* (2021). URL: <http://arxiv.org/abs/2103.14645v1>. 13
- [HXL*20] HUANG Z., XU Y., LASSNER C., LI H., TUNG T.: Arch: Animatable reconstruction of clothed humans. In *Proceedings of the IEEE/CVF Conference on Computer Vision and Pattern Recognition (CVPR)* (2020). URL: <http://arxiv.org/abs/2004.04572v2>. 11, 15, 16
- [HXS*21] HE T., XU Y., SAITO S., SOATTO S., TUNG T.: Arch++: Animation-ready clothed human reconstruction revisited. In *Proceedings of the IEEE International Conference on Computer Vision (ICCV)* (2021). URL: <http://arxiv.org/abs/2108.07845v1>. 16
- [HZ03] HARTLEY R., ZISSERMAN A.: *Multiple View Geometry in Computer Vision*, 2 ed. Cambridge University Press, New York, NY, USA, 2003. 8
- [HZJ*21] HONG Y., ZHANG J., JIANG B., GUO Y., LIU L., BAO H.: Stereopifu: Depth aware clothed human digitization via stereo vision. In *Proceedings of the IEEE/CVF Conference on Computer Vision and Pattern Recognition (CVPR)* (2021). URL: <http://arxiv.org/abs/2104.05289v2>. 15
- [HZRS16] HE K., ZHANG X., REN S., SUN J.: Deep residual learning for image recognition. In *Proceedings of the IEEE Conference on Computer Vision and Pattern Recognition (CVPR)* (2016), pp. 770–778. 4, 12
- [IG21] IZZO D., GOMEZ P.: Geodesy of irregular small bodies via neural density fields: geodesynets. *arXiv preprint arXiv:2105.13031* (2021). URL: <http://arxiv.org/abs/2105.13031v1>. 8, 20
- [ILK21] IBING M., LIM I., KOBELT L.: 3d shape generation with grid-based implicit functions. In *Proceedings of the IEEE/CVF Conference on Computer Vision and Pattern Recognition (CVPR)* (June 2021), pp. 13559–13568. 7
- [Isi21] ISIK B.: Neural 3d scene compression via model compression. *arXiv preprint arXiv:2105.03120* (2021). URL: <http://arxiv.org/abs/2105.03120v1>. 19
- [Izze17] ISOLA P., ZHU J.-Y., ZHOU T., EFROS A. A.: Image-to-image translation with conditional adversarial networks. In *Proc. CVPR* (2017), pp. 1125–1134. 17
- [JA21] JANG W., AGAPITO L.: Codenerf: Disentangled neural radiance fields for object categories. In *Proceedings of the IEEE International Conference on Computer Vision (ICCV)* (2021). URL: <http://arxiv.org/abs/2109.01750v1>. 5
- [JAC*21] JEONG Y., AHN S., CHOY C., ANANDKUMAR A., CHO M., PARK J.: Self-calibrating neural radiance fields. In *Proceedings of the IEEE International Conference on Computer Vision (ICCV)* (2021). 18
- [JGH18] JACOT A., GABRIEL F., HONGLER C.: Neural tangent kernel: Convergence and generalization in neural networks. *arXiv preprint arXiv:1806.07572* (2018). 9
- [JK20] JAGTAP A. D., KARNIADAKIS G. E.: Extended physics-informed neural networks (xpinn): A generalized space-time domain decomposition based deep learning framework for nonlinear partial differential equations. *Communications in Computational Physics* 28, 5 (2020), 2002–2041. 7
- [JMD*07] JOSHI P., MEYER M., DE ROSE T., GREEN B., SANOCKI T.: Harmonic coordinates for character articulation. *ACM Transactions on Graphics (TOG)* 26, 3 (2007), 71–es. 7
- [JSM*20] JIANG C., SUD A., MAKADIA A., HUANG J., NIESSNER M., FUNKHOUSER T., ET AL.: Local implicit grid representations for 3d scenes. In *Proc. CVPR* (2020), pp. 6001–6010. 5, 12
- [JZS*21] JIANG Z., ZHU Y., SVETLIK M., FANG K., ZHU Y.: Synergies between affordance and geometry: 6-dof grasp detection via implicit representations. In *Proceedings of Robotics: Science and Systems* (2021). URL: <http://arxiv.org/abs/2104.01542v2>. 18
- [KA03] KIM T., ADALI T.: Approximation by fully complex multilayer perceptrons. *Neural computation* 15, 7 (2003), 1641–1666. 3
- [Kaj86] KAJIYA J. T.: The rendering equation. In *Proceedings of the 13th annual conference on Computer graphics and interactive techniques* (1986), pp. 143–150. 8, 14
- [KAL*21] KARRAS T., AITTALA M., LAINE S., HÄRKÖNEN E., HELSTEN J., LEHTINEN J., AILA T.: Alias-free generative adversarial networks. *Proc. NeurIPS* (2021). 2, 16
- [KH84] KAJIYA J. T., HERZEN B. P. V.: Ray tracing volume densities. *ACM SIGGRAPH computer graphics* 18, 3 (1984), 165–174. 8, 14
- [KJJ*21] KELLNHOFFER P., JEBE L., JONES A., SPICER R., PULLI K., WETZSTEIN G.: Neural lumigraph rendering. In *Proceedings of the IEEE/CVF Conference on Computer Vision and Pattern Recognition (CVPR)* (2021). URL: <http://arxiv.org/abs/2103.11571v1>. 13
- [KKCF21] KWON Y., KIM D., CEYLAN D., FUCHS H.: Neural human performer: Learning generalizable radiance fields for human performance rendering. In *Advances in Neural Information Processing Systems (NeurIPS)* (2021), Curran Associates, Inc. URL: <http://arxiv.org/abs/2109.07448v1>. 16
- [KKL*21] KARNIADAKIS G. E., KEVREKIDIS I. G., LU L., PERDIKARIS P., WANG S., YANG L.: Physics-informed machine learning. *Nature Reviews Physics* 3, 6 (2021), 422–440. 3, 9
- [KOWD21] KASTEN Y., OFRI D., WANG O., DEKEL T.: Layered neural atlases for consistent video editing. *ACM Transactions on Graphics (TOG)* (2021). URL: <http://arxiv.org/abs/2109.11418v1>. 17
- [KS01] KAK A. C., SLANEY M.: *Front Matter*. SIAM, 2001, pp. i–xiv. URL: <https://epubs.siam.org/doi/abs/10.1137/1.9780898719277.fm>, doi:10.1137/1.9780898719277.fm. 19
- [KS15] KIM D. I., SUKHATME G. S.: Interactive affordance map building for a robotic task. In *2015 IEEE/RSJ International Conference on Intelligent Robots and Systems (IROS)* (2015), pp. 4581–4586. doi:10.1109/IROS.2015.7354029. 18
- [KSW20] KOHLI A., SITZMANN V., WETZSTEIN G.: Semantic implicit neural scene representations with semi-supervised training. In *International Conference on 3D Vision (3DV)* (2020), IEEE. URL: <http://arxiv.org/abs/2003.12673v2>. 13
- [KSZ*21] KOSIOREK A. R., STRATHMANN H., ZORAN D., MORENO P., SCHNEIDER R., MOKRA S., REZENDE D. J.: Nerf-vae: A geometry aware 3d scene generative model. *arXiv preprint arXiv:2104.00587* (2021). URL: <http://arxiv.org/abs/2104.00587v1>. 13
- [KYZ*20] KARUNRATANAKUL K., YANG J., ZHANG Y., BLACK M., MUANDET K., TANG S.: Grasping field: Learning implicit representations for human grasps. In *International Conference on 3D Vision (3DV)* (2020), IEEE. URL: <http://arxiv.org/abs/2008.04451v3>. 16, 18
- [LBB*17] LI T., BOLKART T., BLACK M. J., LI H., ROMERO J.: Learning a model of facial shape and expression from 4d scans. *ACM Trans. Graph.* 36, 6 (2017), 194–1. 15
- [LBH15] LECUN Y., BENGIO Y., HINTON G.: Deep learning. *nature* 521, 7553 (2015), 436–444. 3
- [LEC*20] LEVINSON J., ESTEVES C., CHEN K., SNAVELY N., KANAZAWA A., ROSTAMIZADEH A., MAKADIA A.: An analysis of svd for deep rotation estimation. *arXiv preprint arXiv:2006.14616* (2020). 18

- [LEM91] LEMMON M.: 2-degree-of-freedom robot path planning using cooperative neural fields. *Neural Computation* 3, 3 (1991), 350–362. 18
- [LEM92] LEMMON M.: Oscillatory neural fields for globally optimal path planning. In *Advances in Neural Information Processing Systems* (1992), Moody J., Hanson S., Lippmann R. P., (Eds.), vol. 4, Morgan-Kaufmann. URL: <https://proceedings.neurips.cc/paper/1991/file/c9892a989183de32e976c6f04e700201-Paper.pdf>. 3, 18
- [LGL*20] LIU L., GU J., LIN K. Z., CHUA T.-S., THEOBALT C.: Neural sparse voxel fields. In *Proceedings of the European Conference on Computer Vision (ECCV)* (2020). URL: <http://arxiv.org/abs/2007.11571v2>. 5, 6, 7, 11, 13
- [LHR*21] LIU L., HABERMANN M., RUDNEV V., SARKAR K., GU J., THEOBALT C.: Neural actor: Neural free-view synthesis of human actors with pose control. *ACM Transactions on Graphics (TOG)* (2021). URL: <http://arxiv.org/abs/2106.02019v1>. 10, 16
- [LJLB21] LU Y., JIANG K., LEVINE J. A., BERGER M.: Compressive neural representations of volumetric scalar fields. URL: <http://arxiv.org/abs/2104.04523v1>. 19
- [LLS*21] LI Y., LI S., SITZMANN V., AGRAWAL P., TORRALBA A.: 3d neural scene representations for visuomotor control. In *Proceedings of Robotics: Science and Systems* (2021). URL: <http://arxiv.org/abs/2107.04004v1>. 5, 18
- [LLYX21] LIU C., LI Z., YUAN J., XU Y.: Neulf: Efficient novel view synthesis with neural 4d light field. *arXiv preprint arXiv:2105.07112* (2021). URL: <http://arxiv.org/abs/2105.07112v4>. 14
- [LMR*15] LOPER M., MAHMOOD N., ROMERO J., PONS-MOLL G., BLACK M. J.: Smpl: A skinned multi-person linear model. *ACM transactions on graphics (TOG)* 34, 6 (2015), 1–16. 11, 16
- [LMTL21] LIN C.-H., MA W.-C., TORRALBA A., LUCEY S.: Barf: Bundle-adjusting neural radiance fields. In *Proceedings of the IEEE International Conference on Computer Vision (ICCV)* (2021). URL: <http://arxiv.org/abs/2104.06405v2>. 9, 13, 18
- [LMW21] LINDELL D. B., MARTEL J. N. P., WETZSTEIN G.: Autoint: Automatic integration for fast neural volume rendering. In *Proceedings of the IEEE/CVF Conference on Computer Vision and Pattern Recognition (CVPR)* (2021). URL: <http://arxiv.org/abs/2012.01714v2>. 8, 10
- [LNSW21] LI Z., NIKLAUS S., SNAVELY N., WANG O.: Neural scene flow fields for space-time view synthesis of dynamic scenes. In *Proceedings of the IEEE/CVF Conference on Computer Vision and Pattern Recognition (CVPR)* (2021). URL: <http://arxiv.org/abs/2011.13084v3>. 10, 11, 15
- [LQCA21] LONG K., QIAN C., CORTÉS J., ATANASOV N.: Learning barrier functions with memory for robust safe navigation. *IEEE Robotics and Automation Letters* 6, 3 (2021), 4931–4938. 18
- [LSO4] LIM W. P., SHAMSUDDIN S. M.: *3D Object Reconstruction and Representation Using Neural Networks*. Universiti Teknologi Malaysia, 2004. 11
- [LSCL19] LIU S., SAITO S., CHEN W., LI H.: Learning to infer implicit surfaces without 3d supervision. In *Advances in Neural Information Processing Systems (NeurIPS)* (2019), Curran Associates, Inc. URL: <http://arxiv.org/abs/1911.00767v1>. 8, 13
- [LSS*19] LOMBARDI S., SIMON T., SARAGIH J., SCHWARTZ G., LEHRMANN A., SHEIKH Y.: Neural volumes: Learning dynamic renderable volumes from images. *ACM Transactions on Graphics (TOG)* (2019). URL: <http://arxiv.org/abs/1906.07751v1>, doi: 10.1145/3306346.3323020. 3, 7, 8, 13
- [LSZ*21] LI T., SLAVCHEVA M., ZOLLHOEFER M., GREEN S., LASSNER C., KIM C., SCHMIDT T., LOVEGROVE S., GOESELE M., LV Z.: Neural 3d video synthesis. *arXiv preprint arXiv:2103.02597* (2021). URL: <http://arxiv.org/abs/2103.02597v1>. 15, 19
- [LTW*21] LI N., THAPA S., WHYTE C., REED A., JAYASURIYA S., YE J.: Unsupervised non-rigid image distortion removal via grid deformation. In *Proceedings of the IEEE International Conference on Computer Vision (ICCV)* (2021). 17
- [LW19] LITWIN G., WOLF L.: Deep meta functionals for shape representation. In *Proceedings of the IEEE International Conference on Computer Vision (ICCV)* (2019). URL: <http://arxiv.org/abs/1908.06277v1>. 12
- [LWL20] LIN C.-H., WANG C., LUCEY S.: Sdf-srn: Learning signed distance 3d object reconstruction from static images. In *Advances in Neural Information Processing Systems (NeurIPS)* (2020), Curran Associates, Inc. URL: <http://arxiv.org/abs/2010.10505v1>. 13
- [LXS*20] LI R., XIU Y., SAITO S., HUANG Z., OLSZEWSKI K., LI H.: Monocular real-time volumetric performance capture. In *Proceedings of the European Conference on Computer Vision (ECCV)* (2020). URL: <http://arxiv.org/abs/2007.13988v1>. 15
- [LYP*20] LI Z., YU T., PAN C., ZHENG Z., LIU Y.: Robust 3d self-portraits in seconds. In *Proceedings of the IEEE/CVF Conference on Computer Vision and Pattern Recognition (CVPR)* (2020). URL: <http://arxiv.org/abs/2004.02460v1>. 15
- [LZP*20] LIU S., ZHANG Y., PENG S., SHI B., POLLEFEYS M., CUI Z.: Dist: Rendering deep implicit signed distance function with differentiable sphere tracing. In *Proceedings of the IEEE/CVF Conference on Computer Vision and Pattern Recognition (CVPR)* (2020). URL: <http://arxiv.org/abs/1911.13225v2>. 7, 13
- [LZZ*21] LIU S., ZHANG X., ZHANG Z., ZHANG R., ZHU J.-Y., RUSSELL B.: Editing conditional radiance fields. *arXiv preprint arXiv:2105.06466* (2021). URL: <http://arxiv.org/abs/2105.06466v2>. 5, 11, 12
- [MCL*21] MENG Q., CHEN A., LUO H., WU M., SU H., XU L., HE X., YU J.: Gnerf: Gan-based neural radiance field without posed camera. *arXiv preprint arXiv:2103.15606* (2021). URL: <http://arxiv.org/abs/2103.15606v3>. 18
- [McM02] MCMULLIN E.: The origins of the field concept in physics. *Physics in Perspective* 4, 1 (2002), 13–39. 2
- [MDH*20] MCGUIRE M., DORSEY J., HAINES E., HUGHES J. F., MARSCHNER S., PHARR M., SHIRLEY P.: A taxonomy of bidirectional scattering distribution function lobes for rendering engineers. In *MAM@ EGSR* (2020), pp. 25–28. 14
- [MEJ*21] MURPHY K., ESTEVES C., JAMPANI V., RAMALINGAM S., MAKADIA A.: Implicit-pdf: Non-parametric representation of probability distributions on the rotation manifold. In *International Conference on Machine Learning (ICML)* (2021), PMLR. URL: <http://arxiv.org/abs/2106.05965v1>. 18
- [MGB*21] MEHTA I., GHARBI M., BARNES C., SHECHTMAN E., RAMAMOORTHY R., CHANDRAKER M.: Modulated periodic activations for generalizable local functional representations. In *Proceedings of the IEEE International Conference on Computer Vision (ICCV)* (2021). URL: <http://arxiv.org/abs/2104.03960v1>. 5, 6
- [MLL*21] MARTEL J. N. P., LINDELL D. B., LIN C. Z., CHAN E. R., MONTEIRO M., WETZSTEIN G.: Acorn: Adaptive coordinate networks for neural scene representation. *ACM Transactions on Graphics (TOG)* (2021). URL: <http://arxiv.org/abs/2105.02788v1>. 6, 7, 19
- [MMNM21] MOSELEY B., MARKHAM A., NISSEN-MEYER T.: Finite basis physics-informed neural networks (fbpinns): a scalable domain decomposition approach for solving differential equations. *arXiv preprint arXiv:2107.07871* (2021). URL: <http://arxiv.org/abs/2107.07871v1>. 7
- [MOB*21] MEISTER D., OGAKI S., BENTHIN C., DOYLE M. J., GUTHE M., BITTNER J.: A survey on bounding volume hierarchies for ray tracing. In *Computer Graphics Forum* (2021), vol. 40, Wiley Online Library, pp. 683–712. 6
- [MON*19] MESCHEDER L., OECHSLE M., NIEMEYER M., NOWOZIN S., GEIGER A.: Occupancy networks: Learning 3d reconstruction in

- function space. In *Proceedings of the IEEE/CVF Conference on Computer Vision and Pattern Recognition (CVPR)* (2019). URL: <http://arxiv.org/abs/1812.03828v2>. 2, 12, 16, 19
- [MQK*21] MU J., QIU W., KORTYLEWSKI A., YUILLE A., VASCONCELOS N., WANG X.: A-sdf: Learning disentangled signed distance functions for articulated shape representation. *arXiv preprint arXiv:2104.07645* (2021). URL: <http://arxiv.org/abs/2104.07645v1>. 5, 11
- [MS15] MATURANA D., SCHERER S.: Voxnet: A 3d convolutional neural network for real-time object recognition. In *2015 IEEE/RSJ International Conference on Intelligent Robots and Systems (IROS)* (2015), pp. 922–928. doi:10.1109/IROS.2015.7353481. 4
- [MSOC*19] MILDENHALL B., SRINIVASAN P. P., ORTIZ-CAYON R., KALANTARI N. K., RAMAMOORTHY R., NG R., KAR A.: Local light field fusion: Practical view synthesis with prescriptive sampling guidelines. *ACM Transactions on Graphics (TOG)* (2019). 19
- [MSS*21] MA S., SIMON T., SARAGIH J., WANG D., LI Y., TORRE F. D. L., SHEIKH Y.: Pixel codec avatars. In *Proceedings of the IEEE/CVF Conference on Computer Vision and Pattern Recognition (CVPR)* (2021). URL: <http://arxiv.org/abs/2104.04638v1>. 17
- [MST*20] MILDENHALL B., SRINIVASAN P. P., TANCIK M., BARON J. T., RAMAMOORTHY R., NG R.: Nerf: Representing scenes as neural radiance fields for view synthesis. In *Proceedings of the European Conference on Computer Vision (ECCV)* (2020). URL: <http://arxiv.org/abs/2003.08934v2>. 2, 7, 8, 9, 10, 13, 20
- [MZBT21] MIHAJLOVIC M., ZHANG Y., BLACK M. J., TANG S.: Leap: Learning articulated occupancy of people. In *Proceedings of the IEEE/CVF Conference on Computer Vision and Pattern Recognition (CVPR)* (2021). URL: <http://arxiv.org/abs/2104.06849v1>. 11, 16
- [NBB21] NAM S., BRUBAKER M. A., BROWN M. S.: Neural image representations for multi-image fusion and layer separation. *arXiv preprint arXiv:2108.01199* (2021). URL: <http://arxiv.org/abs/2108.01199v2>. 10, 17
- [NeRa] Nerf at iccv 2021 - frank dellaert. <https://dellaert.github.io/NerF21/>. 3
- [NeRb] Nerf explosion 2020 - frank dellaert. <https://dellaert.github.io/NerF/>. 3
- [NeRc] Nerf: Neural radiance fields - ai research graph - crossminds. <https://crossminds.ai/graphlist/nerf-neural-radiance-fields-ai-research-graph-60708936c8663c4cfa875fc2/>. 3
- [NG21a] NIEMEYER M., GEIGER A.: Campari: Camera-aware decomposed generative neural radiance fields. *arXiv preprint arXiv:2103.17269* (2021). URL: <http://arxiv.org/abs/2103.17269v1>. 17
- [NG21b] NIEMEYER M., GEIGER A.: Giraffe: Representing scenes as compositional generative neural feature fields. In *Proceedings of the IEEE/CVF Conference on Computer Vision and Pattern Recognition (CVPR)* (2021). URL: <http://arxiv.org/abs/2011.12100v2>. 16, 17
- [NMOG19] NIEMEYER M., MESCHEDER L., OECHSLE M., GEIGER A.: Occupancy flow: 4d reconstruction by learning particle dynamics. In *Proceedings of the IEEE International Conference on Computer Vision (ICCV)* (2019), pp. 5379–5389. 2, 10, 11, 15, 16
- [NMOG20] NIEMEYER M., MESCHEDER L., OECHSLE M., GEIGER A.: Differentiable volumetric rendering: Learning implicit 3d representations without 3d supervision. In *Proceedings of the IEEE/CVF Conference on Computer Vision and Pattern Recognition (CVPR)* (2020). URL: <http://arxiv.org/abs/1912.07372v2>. 8, 12, 13
- [NSLH21] NOGUCHI A., SUN X., LIN S., HARADA T.: Neural articulated radiance field. In *Proceedings of the IEEE International Conference on Computer Vision (ICCV)* (2021). URL: <http://arxiv.org/abs/2104.03110v2>. 11
- [NSP*21] NEFF T., STADLBAUER P., PARGER M., KURZ A., MUELLER J. H., CHAITANYA C. R. A., KAPLAYAN A., STEINBERGER M.: Donerf: Towards real-time rendering of compact neural radiance fields using depth oracle networks. *Computer Graphics Forum* (2021). URL: <http://arxiv.org/abs/2103.03231v4>, doi:10.1111/cgf.14340. 8, 13
- [NWH21] NIRKIN Y., WOLF L., HASSNER T.: Hyperseg: Patch-wise hypernetwork/meta-learning for real-time semantic segmentation. In *Proceedings of the IEEE/CVF Conference on Computer Vision and Pattern Recognition (CVPR)* (2021). URL: <http://arxiv.org/abs/2012.11582v2>. 5
- [OF03] OSHER S., FEDKIW R.: Signed distance functions. In *Level set methods and dynamic implicit surfaces*. Springer, 2003, pp. 17–22. 2
- [OMT*21] OST J., MANNAN F., THUEREY N., KNOTT J., HEIDE F.: Neural scene graphs for dynamic scenes. In *Proceedings of the IEEE/CVF Conference on Computer Vision and Pattern Recognition (CVPR)* (2021). URL: <http://arxiv.org/abs/2011.10379v3>. 7, 11
- [OPG21] OECHSLE M., PENG S., GEIGER A.: Unisurf: Unifying neural implicit surfaces and radiance fields for multi-view reconstruction. In *Proceedings of the IEEE International Conference on Computer Vision (ICCV)* (2021). URL: <http://arxiv.org/abs/2104.10078v1>. 9, 13
- [PBD*10] PARKER S. G., BIGLER J., DIETRICH A., FRIEDRICH H., HOBEROCK J., LUEBKE D., MCALLISTER D., MCGUIRE M., MORLEY K., ROBISON A., ET AL.: Optix: a general purpose ray tracing engine. *Acm transactions on graphics (tog)* 29, 4 (2010), 1–13. 6
- [PBT*21] PALAFOX P., BOZIC A., THIES J., NIESSNER M., DAI A.: Npms: Neural parametric models for 3d deformable shapes. In *Proceedings of the IEEE International Conference on Computer Vision (ICCV)* (2021). URL: <http://arxiv.org/abs/2104.00702v2>. 10, 16
- [PCPMN21] PUMAROLA A., CORONA E., PONS-MOLL G., MORENO-NOGUER F.: D-nerf: Neural radiance fields for dynamic scenes. In *Proceedings of the IEEE/CVF Conference on Computer Vision and Pattern Recognition (CVPR)* (2021). URL: <http://arxiv.org/abs/2011.13961v1>. 10, 15
- [PDW*21] PENG S., DONG J., WANG Q., ZHANG S., SHUAI Q., BAO H., ZHOU X.: Animatable neural radiance fields for human body modeling. In *Proceedings of the IEEE International Conference on Computer Vision (ICCV)* (2021). URL: <http://arxiv.org/abs/2105.02872v1>. 16
- [PFS*19] PARK J. J., FLORENCE P., STRAUB J., NEWCOMBE R., LOVEGROVE S.: DeepSDF: Learning continuous signed distance functions for shape representation. In *Proceedings of the IEEE/CVF Conference on Computer Vision and Pattern Recognition (CVPR)* (2019). URL: <http://arxiv.org/abs/1901.05103v1>. 2, 5, 9, 12, 19, 20
- [PH89] PERLIN K., HOFFERT E. M.: Hypertexture. In *Proceedings of the 16th annual conference on Computer graphics and interactive techniques* (1989), pp. 253–262. 8
- [PHP20] PFROMMER S., HALM M., POSA M.: Contactnets: Learning discontinuous contact dynamics with smooth, implicit representations. In *Proceedings of the Conference on Robot Learning (CoRL)* (2020). URL: <http://arxiv.org/abs/2009.11193v2>. 18, 20
- [PJH16] PHARR M., JAKOB W., HUMPHREYS G.: *Physically based rendering: From theory to implementation*. Morgan Kaufmann, 2016. 8
- [PNM*20] PENG S., NIEMEYER M., MESCHEDER L., POLLEFEYS M., GEIGER A.: Convolutional occupancy networks. In *Proceedings of the European Conference on Computer Vision (ECCV)* (2020). URL: <http://arxiv.org/abs/2003.04618v2>. 5, 7, 12
- [PSB*21] PARK K., SINHA U., BARRON J. T., BOUAZIZ S., GOLDMAN D. B., SEITZ S. M., MARTIN-BRUALLA R.: Nerfies: Deformable neural radiance fields. In *Proceedings of the IEEE International Conference on Computer Vision (ICCV)* (2021). URL: <http://arxiv.org/abs/2011.12948v5>. 5, 10, 11, 15

- [PSH*21] PARK K., SINHA U., HEDMAN P., BARRON J. T., BOUAZIZ S., GOLDMAN D. B., MARTIN-BRUALLA R., SEITZ S. M.: Hypernerf: A higher-dimensional representation for topologically varying neural radiance fields. *arXiv preprint arXiv:2106.13228* (2021). URL: <http://arxiv.org/abs/2106.13228v2>. 10, 15
- [PXZ*21] PAN H., XIAO D., ZHANG F., LI X., XU M.: Adaptive weight matrix and phantom intensity learning for computed tomography of chemiluminescence. *Opt. Express* 29, 15 (Jul 2021), 23682–23700. URL: <http://www.opticsexpress.org/abstract.cfm?URI=oe-29-15-23682>, doi:10.1364/OE.427459. 19
- [PZX*21] PENG S., ZHANG Y., XU Y., WANG Q., SHUAI Q., BAO H., ZHOU X.: Neural body: Implicit neural representations with structured latent codes for novel view synthesis of dynamic humans. In *Proceedings of the IEEE/CVF Conference on Computer Vision and Pattern Recognition (CVPR)* (2021). URL: <http://arxiv.org/abs/2012.15838v2>. 6, 7, 16
- [QMGR20] QI W., MULLAPUDI R. T., GUPTA S., RAMANAN D.: Learning to move with affordance maps. *arXiv preprint arXiv:2001.02364* (2020). 18
- [QSMG17] QI C. R., SU H., MO K., GUIBAS L. J.: Pointnet: Deep learning on point sets for 3d classification and segmentation. In *Proceedings of the IEEE Conference on Computer Vision and Pattern Recognition (CVPR)* (2017), pp. 652–660. 4, 12
- [RBA*19] RAHAMAN N., BARATIN A., ARPIT D., DRAXLER F., LIN M., HAMPRECHT F., BENGIO Y., COURVILLE A.: On the spectral bias of neural networks. In *Proceedings of the 36th International Conference on Machine Learning* (09–15 Jun 2019), Chaudhuri K., Salakhutdinov R., (Eds.), vol. 97 of *Proceedings of Machine Learning Research*, PMLR, pp. 5301–5310. URL: <https://proceedings.mlr.press/v97/rahaman19a.html>. 9
- [RBBJ] REED A., BLANFORD T., BROWN D. C., JAYASURIYA S.: Implicit neural representations for deconvolving sas images. 8, 19, 20
- [RBZ*20] REMPE D., BIRDAL T., ZHAO Y., GOJCIC Z., SRIDHAR S., GUIBAS L. J.: Caspr: Learning canonical spatiotemporal point cloud representations. *arXiv preprint arXiv:2008.02792* (2020). 15
- [RJY*21] REBAIN D., JIANG W., YAZDANI S., LI K., YI K. M., TAGLIASACCHI A.: Derf: Decomposed radiance fields. In *Proceedings of the IEEE/CVF Conference on Computer Vision and Pattern Recognition (CVPR)* (2021). URL: <http://arxiv.org/abs/2011.12490v1>. 6, 7
- [RLS*21] REBAIN D., LI K., SITZMANN V., YAZDANI S., YI K. M., TAGLIASACCHI A.: Deep medial fields. *arXiv preprint arXiv:2106.03804* (2021). URL: <http://arxiv.org/abs/2106.03804v1>. 12
- [RPK] RAISSI M., PERDIKARIS P., KARNIADAKIS G. E.: Physics-informed neural networks: A deep learning framework for solving forward and inverse problems involving nonlinear partial differential equations. *Journal of Computational Physics* 378, 686–707. 7
- [RPK19] RAISSI M., PERDIKARIS P., KARNIADAKIS G. E.: Physics-informed neural networks: A deep learning framework for solving forward and inverse problems involving nonlinear partial differential equations. *Journal of Computational Physics* 378 (2019), 686–707. 3, 20
- [RPLG21] REISER C., PENG S., LIAO Y., GEIGER A.: Kilonerf: Speeding up neural radiance fields with thousands of tiny mlps. In *Proceedings of the IEEE International Conference on Computer Vision (ICCV)* (2021). URL: <http://arxiv.org/abs/2103.13744v2>. 7, 13
- [RSH*21] REIZENSTEIN J., SHAPOVALOV R., HENZLER P., SBORDONE L., LABATUT P., NOVOTNY D.: Common objects in 3d: Large-scale learning and evaluation of real-life 3d category reconstruction. In *Proceedings of the IEEE/CVF Conference on Computer Vision and Pattern Recognition (CVPR)* (2021). URL: <http://arxiv.org/abs/2109.00512v1>. 13
- [RTE*21] RAMON E., TRIGNER G., ESCUR J., PUMAROLA A., GARCIA J., NIETO X. G., MORENO-NOGUER F.: H3d-net: Few-shot high-fidelity 3d head reconstruction. *arXiv preprint arXiv:2107.12512* (2021). URL: <http://arxiv.org/abs/2107.12512v1>. 2, 5, 15
- [RW80] RUBIN S. M., WHITTED T.: A 3-dimensional representation for fast rendering of complex scenes. In *Proceedings of the 7th annual conference on Computer graphics and interactive techniques* (1980), pp. 110–116. 6
- [RWG*13] REN P., WANG J., GONG M., LIN S., TONG X., GUO B.: Global illumination with radiance regression functions. *ACM Trans. Graph.* 32, 4 (jul 2013). URL: <https://doi.org/10.1145/2461912.2462009>, doi:10.1145/2461912.2462009. 6, 7
- [RZS*21] RAJ A., ZOLLHOEFER M., SIMON T., SARAGIH J., SAITO S., HAYS J., LOMBARDI S.: Pva: Pixel-aligned volumetric avatars. In *Proceedings of the IEEE/CVF Conference on Computer Vision and Pattern Recognition (CVPR)* (2021). URL: <http://arxiv.org/abs/2101.02697v1>. 15
- [Sab88] SABELLA P.: A rendering algorithm for visualizing 3d scalar fields. In *Proceedings of the 15th annual conference on Computer graphics and interactive techniques* (1988), pp. 51–58. 2
- [SAR20] SMITH J. D., AZIZZADENESHELI K., ROSS Z. E.: Eikonet: Solving the eikonal equation with deep neural networks. URL: <http://arxiv.org/abs/2004.00361v3>. 20
- [SC21] SU N. M., CRANDALL D. J.: The affective growth of computer vision. In *Proceedings of the IEEE/CVF Conference on Computer Vision and Pattern Recognition* (2021), pp. 9291–9300. 2, 20
- [SCA19] SBAI O., COUPRIE C., AUBRY M.: Unsupervised image decomposition in vector layers, 2019. [arXiv:1812.05484](https://arxiv.org/abs/1812.05484). 17
- [SCT*20] SITZMANN V., CHAN E. R., TUCKER R., SNAVELY N., WETZSTEIN G.: Metasdf: Meta-learning signed distance functions. In *Advances in Neural Information Processing Systems (NeurIPS)* (2020), Curran Associates, Inc. URL: <http://arxiv.org/abs/2006.09662v1>. 5, 6, 12
- [SDZ*21] SRINIVASAN P. P., DENG B., ZHANG X., TANCIK M., MILDENHALL B., BARRON J. T.: Nerv: Neural reflectance and visibility fields for relighting and view synthesis. In *Proceedings of the IEEE/CVF Conference on Computer Vision and Pattern Recognition (CVPR)* (2021). URL: <http://arxiv.org/abs/2012.03927v1>. 14
- [SF16] SCHÖNBERGER J. L., FRAHM J.-M.: Structure-from-motion revisited. In *Conference on Computer Vision and Pattern Recognition (CVPR)* (2016). 17
- [SFE*20] SUTANTO G., FERNANDEZ I. M. R., ENGLERT P., RAMACHANDRAN R. K., SUKHATME G. S.: Learning equality constraints for motion planning on manifolds. In *Proceedings of the Conference on Robot Learning (CoRL)* (2020). URL: <http://arxiv.org/abs/2009.11852v1>. 18
- [SGZ*21] SHAHAM T. R., GHARBI M., ZHANG R., SHECHTMAN E., MICHAELI T.: Spatially-adaptive pixelwise networks for fast image translation. In *Proceedings of the IEEE/CVF Conference on Computer Vision and Pattern Recognition (CVPR)* (2021). URL: <http://arxiv.org/abs/2012.02992v1>. 17
- [SHN*19] SAITO S., HUANG Z., NATSUME R., MORISHIMA S., KANAZAWA A., LI H.: Pifu: Pixel-aligned implicit function for high-resolution clothed human digitization. In *Proceedings of the IEEE/CVF Conference on Computer Vision and Pattern Recognition (CVPR)* (2019). URL: <http://arxiv.org/abs/1905.05172v3>. 5, 7, 8, 13, 15
- [Sib81] SIBSON R.: A brief description of natural neighbour interpolation. *Interpreting multivariate data* (1981). 7
- [SIE21] SKOROKHODOV I., IGNATYEV S., ELHOSEINY M.: Adversarial generation of continuous images. In *Proceedings of the IEEE/CVF Conference on Computer Vision and Pattern Recognition (CVPR)* (2021). URL: <http://arxiv.org/abs/2011.12026v2>. 6, 16, 17

- [Sit] SITZMANN V.: Awesome implicit representations - a curated list of resources on implicit neural representations. URL: <https://github.com/vsitzmann/awesome-implicit-representations>. 3
- [SJK21] SHUKLA K., JAGTAP A. D., KARNIADAKIS G. E.: Parallel physics-informed neural networks via domain decomposition. *arXiv preprint arXiv:2104.10013* (2021). URL: <http://arxiv.org/abs/2104.10013v3>. 7
- [SJL*21] SUO X., JIANG Y., LIN P., ZHANG Y., WU M., GUO K., XU L.: Neuralhumanfvv: Real-time neural volumetric human performance rendering using rgb cameras. In *Proceedings of the IEEE/CVF Conference on Computer Vision and Pattern Recognition* (2021), pp. 6226–6237. 15
- [SK97] SCHLÜNS K., KLETTE R.: Local and global integration of discrete vector fields. In *Advances in Computer Vision*. Springer, 1997, pp. 149–158. 2
- [SLNG20] SCHWARZ K., LIAO Y., NIEMEYER M., GEIGER A.: Graf: Generative radiance fields for 3d-aware image synthesis. In *Advances in Neural Information Processing Systems (NeurIPS)* (2020), Curran Associates, Inc. URL: <http://arxiv.org/abs/2007.02442v4>. 16
- [SLOD21] SUCAR E., LIU S., ORTIZ J., DAVISON A. J.: imap: Implicit mapping and positioning in real-time. In *Proceedings of the IEEE International Conference on Computer Vision (ICCV)* (2021). URL: <http://arxiv.org/abs/2103.12352v2>. 17, 18
- [SLX*21] SUN Y., LIU J., XIE M., WOHLBERG B., KAMILOV U. S.: Coil: Coordinate-based internal learning for imaging inverse problems. *arXiv preprint arXiv:2102.05181* (2021). URL: <http://arxiv.org/abs/2102.05181v1>. 8, 19
- [SMB*20] SITZMANN V., MARTEL J. N. P., BERGMAN A. W., LINDSELL D. B., WETZSTEIN G.: Implicit neural representations with periodic activation functions. In *Advances in Neural Information Processing Systems (NeurIPS)* (2020), Curran Associates, Inc. URL: <http://arxiv.org/abs/2006.09661v1>. 5, 9, 10, 12, 16, 17, 19, 20
- [SOHW12] SULLIVAN G. J., OHM J.-R., HAN W.-J., WIEGAND T.: Overview of the high efficiency video coding (hevc) standard. *IEEE Transactions on circuits and systems for video technology* 22, 12 (2012), 1649–1668. 18, 19
- [SPX21] SHEN L., PAULY J., XING L.: Nerp: Implicit neural representation learning with prior embedding for sparsely sampled image reconstruction. *arXiv preprint arXiv:ers/2108/2108.10991* (2021). URL: <http://arxiv.org/abs/2108.10991v1>. 7, 8, 19
- [SRF*21] SITZMANN V., REZCHIKOV S., FREEMAN W. T., TENENBAUM J. B., DURAND F.: Light field networks: Neural scene representations with single-evaluation rendering. In *Proc. NeurIPS* (2021). URL: <http://arxiv.org/abs/2106.02634v1>. 5, 14, 19
- [SSSJ20] SAITO S., SIMON T., SARAGIH J., JOO H.: Pifuhd: Multi-level pixel-aligned implicit function for high-resolution 3d human digitization. In *Proceedings of the IEEE/CVF Conference on Computer Vision and Pattern Recognition (CVPR)* (2020). URL: <http://arxiv.org/abs/2004.00452v1>. 7, 15
- [Sta07] STANLEY K. O.: Compositional pattern producing networks: A novel abstraction of development. *Genetic programming and evolvable machines* 8, 2 (2007), 131–162. 17
- [STH*19] SITZMANN V., THIES J., HEIDE F., NIESSNER M., WETZSTEIN G., ZOLLHÖFER M.: Deepvoxels: Learning persistent 3d feature embeddings. In *Proc. Computer Vision and Pattern Recognition (CVPR), IEEE* (2019). 3
- [SWL*21] SHEN S., WANG Z., LIU P., PAN Z., LI R., GAO T., LI S., YU J.: Non-line-of-sight imaging via neural transient fields. *IEEE Transactions on Pattern Analysis and Machine Intelligence* (2021). URL: <http://arxiv.org/abs/2101.00373v3>. 19
- [SYMB21] SAITO S., YANG J., MA Q., BLACK M. J.: Scanimate: Weakly supervised learning of skinned clothed avatar networks. In *Proceedings of the IEEE/CVF Conference on Computer Vision and Pattern Recognition (CVPR)* (2021). URL: <http://arxiv.org/abs/2104.03313v2>. 2, 10, 11, 16
- [SYZR21] SU S.-Y., YU F., ZOLLHÖFER M., RHODIN H.: A-nerf: Surface-free human 3d pose refinement via neural rendering. *arXiv preprint arXiv:2102.06199* (2021). URL: <http://arxiv.org/abs/2102.06199v1>. 11, 16
- [SZPF16] SCHÖNBERGER J. L., ZHENG E., POLLEFEYS M., FRAHM J.-M.: Pixelwise view selection for unstructured multi-view stereo. In *European Conference on Computer Vision (ECCV)* (2016). 17
- [SZW19] SITZMANN V., ZOLLHOFER M., WETZSTEIN G.: Scene representation networks: Continuous 3d-structure-aware neural scene representations. In *Advances in Neural Information Processing Systems (NeurIPS)* (2019), Curran Associates, Inc. URL: <http://arxiv.org/abs/1906.01618v2>. 2, 5, 8, 12, 13, 20
- [SZ*21] SHAO R., ZHANG H., ZHANG H., CAO Y., YU T., LIU Y.: Doublefield: Bridging the neural surface and radiance fields for high-fidelity human rendering. *arXiv preprint arXiv:2106.03798* (2021). URL: <http://arxiv.org/abs/2106.03798v2>. 16
- [TFT*20] TEWARI A., FRIED O., THIES J., SITZMANN V., LOMBARDI S., SUNKAVALLI K., MARTIN-BRUALLA R., SIMON T., SARAGIH J., NIESSNER M., ET AL.: State of the art on neural rendering. In *Computer Graphics Forum* (2020), vol. 39, Wiley Online Library, pp. 701–727. 3
- [TLV21] TSCHERNEZKI V., LARLUS D., VEDALDI A.: Neuraldiff: Segmenting 3d objects that move in egocentric videos. *arXiv preprint arXiv:2110.09936* (2021). 20
- [TLY*21] TAKIKAWA T., LITALIEN J., YIN K., KREIS K., LOOP C., NOWROUZEZHAI D., JACOBSON A., MCGUIRE M., FIDLER S.: Neural geometric level of detail: Real-time rendering with implicit 3d shapes. In *Proceedings of the IEEE/CVF Conference on Computer Vision and Pattern Recognition (CVPR)* (2021). URL: <http://arxiv.org/abs/2101.10994v1>. 7, 12, 19
- [TMW*21] TANCİK M., MILDENHALL B., WANG T., SCHMIDT D., SRINIVASAN P. P., BARRON J. T., NG R.: Learned initializations for optimizing coordinate-based neural representations. In *Proceedings of the IEEE/CVF Conference on Computer Vision and Pattern Recognition (CVPR)* (2021). URL: <http://arxiv.org/abs/2012.02189v2>. 6
- [TSM*20] TANCİK M., SRINIVASAN P. P., MILDENHALL B., FRIDOVICH-KEIL S., RAGHAVAN N., SINGHAL U., RAMAMOORTHY R., BARRON J. T., NG R.: Fourier features let networks learn high frequency functions in low dimensional domains. In *Advances in Neural Information Processing Systems (NeurIPS)* (2020), Curran Associates, Inc. URL: <http://arxiv.org/abs/2006.10739v1>. 9, 13, 16, 17
- [TSTPM21] TIWARI G., SARAFIANOS N., TUNG T., PONS-MOLL G.: Neural-gif: Neural generalized implicit functions for animating people in clothing. In *Proceedings of the IEEE International Conference on Computer Vision (ICCV)* (2021). URL: <http://arxiv.org/abs/2108.08807v2>. 10, 11, 16
- [TTG*20] TRETSCHEK E., TEWARI A., GOLYANIK V., ZOLLHOFER M., STOLL C., THEOBALT C.: Patchnets: Patch-based generalizable deep implicit 3d shape representations. In *Proceedings of the European Conference on Computer Vision (ECCV)* (2020). URL: <http://arxiv.org/abs/2008.01639v2>. 5, 7
- [TTG*21] TRETSCHEK E., TEWARI A., GOLYANIK V., ZOLLHOFER M., LASSNER C., THEOBALT C.: Non-rigid neural radiance fields: Reconstruction and novel view synthesis of a dynamic scene from monocular video. In *Proceedings of the IEEE International Conference on Computer Vision (ICCV)* (2021). URL: <http://arxiv.org/abs/2012.12247v4>. 5, 10, 11, 15
- [TVRF*20] TOLOSANA R., VERA-RODRIGUEZ R., FIERREZ J., MORALES A., ORTEGA-GARCIA J.: Deepfakes and beyond: A survey of face manipulation and fake detection. *Information Fusion* 64 (2020), 131–148. 20

- [TY21] TREVITHICK A., YANG B.: Grf: Learning a general radiance field for 3d representation and rendering. In *Proceedings of the IEEE International Conference on Computer Vision (ICCV)* (2021). URL: <http://arxiv.org/abs/2010.04595v3>. 5, 7, 13
- [VJK21] VICINI D., JAKOB W., KAPLANYAN A.: A non-exponential transmittance model for volumetric scene representations. *ACM Transactions on Graphics (TOG)* 40, 4 (2021), 1–16. 8
- [Wal92] WALLACE G.: The jpeg still picture compression standard. *IEEE Transactions on Consumer Electronics* 38, 1 (1992), xviii–xxxiv. doi: [10.1109/30.125072](https://doi.org/10.1109/30.125072). 18, 19
- [War92] WARD G. J.: Measuring and modeling anisotropic reflection. In *Proceedings of the 19th annual conference on Computer graphics and interactive techniques* (1992), pp. 265–272. 14
- [WBL*21] WANG Z., BAGAUTDINOV T., LOMBARDI S., SIMON T., SARAGIH J., HODGINS J., ZOLLHOFER M.: Learning compositional radiance fields of dynamic human heads. In *Proceedings of the IEEE/CVF Conference on Computer Vision and Pattern Recognition (CVPR)* (2021). URL: <http://arxiv.org/abs/2012.09955v1>. 15
- [WELG21] WANG C., ECKART B., LUCEY S., GALLO O.: Neural trajectory fields for dynamic novel view synthesis. *arXiv preprint arXiv:2105.05994* (2021). URL: <http://arxiv.org/abs/2105.05994v1>. 10, 11
- [WGT21] WANG S., GEIGER A., TANG S.: Locally aware piecewise transformation fields for 3d human mesh registration. In *Proceedings of the IEEE/CVF Conference on Computer Vision and Pattern Recognition (CVPR)* (2021). URL: <http://arxiv.org/abs/2104.08160v1>. 16
- [WLL*21] WANG P., LIU L., LIU Y., THEOBALT C., KOMURA T., WANG W.: Neus: Learning neural implicit surfaces by volume rendering for multi-view reconstruction. In *Proceedings of the Thirtieth International Joint Conference on Artificial Intelligence (IJCAI)* (2021), International Joint Conferences on Artificial Intelligence Organization. URL: <http://arxiv.org/abs/2106.10689v1>. 9, 13
- [WLYT21] WANG P.-S., LIU Y., YANG Y.-Q., TONG X.: Spline positional encoding for learning 3d implicit signed distance fields. In *Proceedings of the Thirtieth International Joint Conference on Artificial Intelligence (IJCAI)* (2021), International Joint Conferences on Artificial Intelligence Organization. URL: <http://arxiv.org/abs/2106.01553v1>. 9
- [WMLT07] WALTER B., MARSCHNER S. R., LI H., TORRANCE K. E.: Microfacet models for refraction through rough surfaces. *Rendering techniques 2007* (2007), 18th. 14
- [WMM*21] WANG S., MIHAJLOVIC M., MA Q., GEIGER A., TANG S.: Metaavatar: Learning animatable clothed human models from few depth images. In *Proceedings of the Thirtieth International Joint Conference on Artificial Intelligence (IJCAI)* (2021), International Joint Conferences on Artificial Intelligence Organization. URL: <http://arxiv.org/abs/2106.11944v1>. 10, 16
- [WPLN*20] WILLIAMS F., PARENT-LEVESQUE J., NOWROUZEZAHRAI D., PANOZZO D., YI K. M., TAGLIASACCHI A.: Voronoinet: General functional approximators with local support. In *Proceedings of the IEEE/CVF Conference on Computer Vision and Pattern Recognition Workshops* (2020), pp. 264–265. 7
- [WPYS21] WIZADWONGSA S., PHONGTHAWEE P., YENPHRAPHAI J., SUWAJANAKORN S.: Nex: Real-time view synthesis with neural basis expansion. In *Proceedings of the IEEE/CVF Conference on Computer Vision and Pattern Recognition (CVPR)* (2021). URL: <http://arxiv.org/abs/2103.05606v2>. 8, 14
- [WSH*19] WANG H., SRIDHAR S., HUANG J., VALENTIN J., SONG S., GUIBAS L. J.: Normalized object coordinate space for category-level 6d object pose and size estimation. In *Proceedings of the IEEE/CVF Conference on Computer Vision and Pattern Recognition* (2019), pp. 2642–2651. 7
- [WTBZ21] WILLIAMS F., TRAGER M., BRUNA J., ZORIN D.: Neural splines: Fitting 3d surfaces with infinitely-wide neural networks. In *Proceedings of the IEEE/CVF Conference on Computer Vision and Pattern Recognition (CVPR)* (2021). URL: <http://arxiv.org/abs/2006.13782v3>. 13
- [WWB*14] WALD I., WOOP S., BENTHIN C., JOHNSON G. S., ERNST M.: Embree: a kernel framework for efficient cpu ray tracing. *ACM Transactions on Graphics (TOG)* 33, 4 (2014), 1–8. 6
- [WWX*21] WANG Z., WU S., XIE W., CHEN M., PRISACARIU V. A.: Nerf-: Neural radiance fields without known camera parameters. *arXiv preprint arXiv:2102.07064* (2021). URL: <http://arxiv.org/abs/2102.07064v3>. 13, 18
- [WWZ*21] WANG Z., WANG L., ZHAO F., WU M., XU L., YU J.: Mirrornerf: One-shot neural portrait radiance field from multi-mirror catadioptric imaging. *arXiv preprint arXiv:2104.02607* (2021). URL: <http://arxiv.org/abs/2104.02607v2>. 10
- [XHKK21] XIAN W., HUANG J.-B., KOPF J., KIM C.: Space-time neural irradiance fields for free-viewpoint video. In *Proceedings of the IEEE/CVF Conference on Computer Vision and Pattern Recognition (CVPR)* (2021). URL: <http://arxiv.org/abs/2011.12950v2>. 11, 15
- [XWC*19] XU Q., WANG W., CEYLAN D., MECH R., NEUMANN U.: Disn: Deep implicit surface network for high-quality single-view 3d reconstruction. In *Advances in Neural Information Processing Systems (NeurIPS)* (2019), Curran Associates, Inc. URL: <http://arxiv.org/abs/1905.10711v2>. 13
- [YCFB*21] YEN-CHEN L., FLORENCE P., BARRON J. T., RODRIGUEZ A., ISOLA P., LIN T.-Y.: iNeRF: Inverting neural radiance fields for pose estimation. In *IEEE/RSJ International Conference on Intelligent Robots and Systems (IROS)* (2021). 13, 18
- [YFST18] YANG Y., FENG C., SHEN Y., TIAN D.: Foldingnet: Point cloud auto-encoder via deep grid deformation. In *Proceedings of the IEEE/CVF Conference on Computer Vision and Pattern Recognition (CVPR)* (2018). URL: <http://arxiv.org/abs/1712.07262v2>. 12
- [YGKL21] YARIV L., GU J., KASTEN Y., LIPMAN Y.: Volume rendering of neural implicit surfaces. In *Advances in Neural Information Processing Systems (NeurIPS)* (2021), Curran Associates, Inc. URL: <http://arxiv.org/abs/2106.12052v1>. 9, 13
- [YKM*20] YARIV L., KASTEN Y., MORAN D., GALUN M., ATZMON M., BASRI R., LIPMAN Y.: Multiview neural surface reconstruction by disentangling geometry and appearance. In *Advances in Neural Information Processing Systems (NeurIPS)* (2020), Curran Associates, Inc. URL: <http://arxiv.org/abs/2003.09852v3>. 8, 12, 13, 15
- [YLB*20] YANG Z., LITANY O., BIRDAL T., SRIDHAR S., GUIBAS L.: Continuous geodesic convolutions for learning on 3d shapes, 2020. [arXiv:2002.02506](https://arxiv.org/abs/2002.02506). 16
- [YLSL21] YUAN W., LV Z., SCHMIDT T., LOVEGROVE S.: Star: Self-supervised tracking and reconstruction of rigid objects in motion with neural rendering. In *Proceedings of the IEEE/CVF Conference on Computer Vision and Pattern Recognition (CVPR)* (2021). URL: <http://arxiv.org/abs/2101.01602v1>. 15
- [YLT*21] YU A., LI R., TANCIK M., LI H., NG R., KANAZAWA A.: Plenotrees for real-time rendering of neural radiance fields. *Proc. ICCV* (2021). 13
- [YTB*21] YENAMANDRA T., TEWARI A., BERNARD F., SEIDEL H.-P., ELGHARIB M., CREMERS D., THEOBALT C.: i3dmm: Deep implicit 3d morphable model of human heads. In *Proceedings of the IEEE/CVF Conference on Computer Vision and Pattern Recognition (CVPR)* (2021). URL: <http://arxiv.org/abs/2011.14143v1>. 2, 10, 15
- [YWC*21] YANG M., WEN Y., CHEN W., CHEN Y., JIA K.: Deep optimized priors for 3d shape modeling and reconstruction. In *Proceedings of the IEEE/CVF Conference on Computer Vision and Pattern Recognition (CVPR)* (2021). URL: <http://arxiv.org/abs/2012.07241v1>. 5, 12

- [YWM*21] YANG Z., WANG S., MANIVASAGAM S., HUANG Z., MA W.-C., YAN X., YUMER E., URTASUN R.: S3: Neural shape, skeleton, and skinning fields for 3d human modeling. In *Proceedings of the IEEE/CVF Conference on Computer Vision and Pattern Recognition (CVPR)* (2021). URL: <http://arxiv.org/abs/2101.06571v1>. 15
- [YYTK21] YU A., YE V., TANCIK M., KANAZAWA A.: pixelnerf: Neural radiance fields from one or few images. In *Proceedings of the IEEE/CVF Conference on Computer Vision and Pattern Recognition (CVPR)* (2021). URL: <http://arxiv.org/abs/2012.02190v3>. 5, 13
- [YZG*21] YU T., ZHENG Z., GUO K., LIU P., DAI Q., LIU Y.: Function4d: Real-time human volumetric capture from very sparse consumer rgbd sensors. In *Proceedings of the IEEE/CVF Conference on Computer Vision and Pattern Recognition* (2021), pp. 5746–5756. 15
- [ZBDB20a] ZHONG E. D., BEPLER T., DAVIS J. H., BERGER B.: Reconstructing continuous distributions of 3d protein structure from cryo-em images. *Proc. ICLR* (2020). 9
- [ZBDB20b] ZHONG E. D., BEPLER T., DAVIS J. H., BERGER B.: Reconstructing continuous distributions of 3d protein structure from cryo-em images. In *International Conference on Learning Representations* (2020). URL: <http://arxiv.org/abs/1909.05215v3>. 13, 20
- [ZBL*19] ZHOU Y., BARNES C., LU J., YANG J., LI H.: On the continuity of rotation representations in neural networks. In *Proceedings of the IEEE/CVF Conference on Computer Vision and Pattern Recognition* (2019), pp. 5745–5753. 18
- [ZBW*20] ZHENG Q., BABAEI V., WETZSTEIN G., SEIDEL H.-P., ZWICKER M., SINGH G.: Neural light field 3d printing. *ACM Transactions on Graphics (TOG)* 39, 6 (2020), 1–12. 19
- [ZIL*21] ZANG G., IDOUGHI R., LI R., WONKA P., HEIDRICH W.: Intratomo: Self-supervised learning-based tomography via sinogram synthesis and prediction. In *Proceedings of the IEEE International Conference on Computer Vision (ICCV)* (2021), IEEE. 8, 19
- [ZLCT21] ZEHNDER J., LI Y., COROS S., THOMASZEWSKI B.: Ntopo: Mesh-free topology optimization using implicit neural representations. *arXiv preprint arXiv:2102.10782* (2021). URL: <http://arxiv.org/abs/2102.10782v1>. 20
- [ZLW*21] ZHANG K., LUAN F., WANG Q., BALA K., SNAVELY N.: Physg: Inverse rendering with spherical gaussians for physics-based material editing and relighting. In *Proceedings of the IEEE/CVF Conference on Computer Vision and Pattern Recognition (CVPR)* (2021). URL: <http://arxiv.org/abs/2104.00674v1>. 14
- [ZLY*21] ZHANG J., LIU X., YE X., ZHAO F., ZHANG Y., WU M., ZHANG Y., XU L., YU J.: Editable free-viewpoint video using a layered neural representation. *ACM Transactions on Graphics (TOG)* (2021). URL: <http://arxiv.org/abs/2104.14786v1>, doi: 10.1145/3450626.3459756. 6, 7, 10, 11
- [ZRL21] ZHENG J., RAMASINGHE S., LUCEY S.: Rethinking positional encoding. *arXiv preprint arXiv:2107.02561* (2021). URL: <http://arxiv.org/abs/2107.02561v2>. 9
- [ZRSK20] ZHANG K., RIEGLER G., SNAVELY N., KOLTUN V.: Nerf++: Analyzing and improving neural radiance fields. *arXiv preprint arXiv:2010.07492* (2020). URL: <http://arxiv.org/abs/2010.07492v2>. 13
- [ZS20] ZHANG Z., SCARAMUZZA D.: Fisher information field: an efficient and differentiable map for perception-aware planning. *arXiv preprint arXiv:2008.03324* (2020). 18
- [ZSD*21] ZHANG X., SRINIVASAN P. P., DENG B., DEBEVEC P., FREEMAN W. T., BARRON J. T.: Nerfactor: Neural factorization of shape and reflectance under an unknown illumination. *arXiv preprint arXiv:2106.01970* (2021). URL: <http://arxiv.org/abs/2106.01970v1>. 12, 14
- [ZSG*18] ZOLLHÖFER M., STOTKO P., GÖRLITZ A., THEOBALT C., NIESSNER M., KLEIN R., KOLB A.: State of the art on 3d reconstruction with rgb-d cameras. In *Computer graphics forum* (2018), vol. 37, Wiley Online Library, pp. 625–652. 3
- [ZYLD21] ZHENG Z., YU T., LIU Y., DAI Q.: Pamir: Parametric model-conditioned implicit representation for image-based human reconstruction. *IEEE Transactions on Pattern Analysis and Machine Intelligence* (2021). 15, 16